Proterozoic crustal evolution of central East Antarctica: Age and isotopic evidence from glacial igneous clasts, and links with Australia and Laurentia

John W. Goodge, C. Mark Fanning, Christopher M. Fisher, Jeffrey D. Vervoort

PII: S0301-9268(17)30089-X
DOI: http://dx.doi.org/10.1016/j.precamres.2017.07.026
Reference: PRECAM 4836

To appear in: *Precambrian Research*

Received Date: 17 February 2017
Revised Date: 2 July 2017
Accepted Date: 18 July 2017

Please cite this article as: J.W. Goodge, C. Mark Fanning, C.M. Fisher, J.D. Vervoort, Proterozoic crustal evolution of central East Antarctica: Age and isotopic evidence from glacial igneous clasts, and links with Australia and Laurentia, *Precambrian Research* (2017), doi: http://dx.doi.org/10.1016/j.precamres.2017.07.026

Proterozoic crustal evolution of central East Antarctica: Age and isotopic evidence from glacial igneous clasts, and links with Australia and Laurentia

John W. Goodge [1]*, C. Mark Fanning[2], Christopher M. Fisher[3]† and Jeffrey D. Vervoort[3]

[1] Department of Earth and Environmental Sciences, University of Minnesota, Duluth, MN 55812 USA (correspondence: jgoodge@d.umn.edu)

[2] Research School of Earth Sciences, Australian National University, Canberra, ACT 0200 Australia (mark.fanning@anu.edu.au)

[3] School of the Environment, Washington State University, Pullman, WA 99164, USA (vervoort@wsu.edu, cmfisher@ualberta.ca)

Submitted to *Precambrian Research*

* corresponding author; † present address: Department of Earth & Atmospheric Sciences, University of Alberta, Edmonton, Alberta, Canada T6G 2E3

Abstract. Rock clasts entrained in glacial deposits sourced from the continental interior of Antarctica provide an innovative means to determine the age and composition of ice-covered crust. Zircon U-Pb ages from a suite of granitoid clasts collected in glacial catchments draining central East Antarctica through the Transantarctic Mountains show that crust in this region was formed by a series of magmatic events at ~2.01, 1.88-1.85, ~1.79, ~1.57, 1.50-1.41, and 1.20-1.06 Ga. The dominant granitoid populations are ca. 1.85, 1.45 and 1.20-1.06 Ga. None of these igneous ages are known from limited outcrop in the region. In addition to defining a previously unrecognized geologic history, zircon O and Hf isotopic compositions from this suite have: (1) mantle-like $\delta^{18}O$ signatures (4.0-4.5‰) and near-chondritic Hf-isotope compositions (ε_{Hf} ~ +1.5) for granitoids of ~2.0 Ga age; (2) mostly crustal $\delta^{18}O$ (6.0-8.5‰) and variable Hf-isotope compositions (ε_{Hf} = -6 to +5) in rocks with ages of ~1.88-1.85, ~1.79 and ~1.57 Ga, in which the ~1.88-1.79 Ga granitoids require involvement of older crust; (3) mostly juvenile isotopic signatures with low, mantle-like $\delta^{18}O$ (~4-5‰) and radiogenic Hf-isotope signatures (ε_{Hf} = +6 to +10) in rocks of 1.50-1.41 Ga age, with some showing crustal sources or evidence of alteration; and (4) mixed crustal and mantle $\delta^{18}O$ signatures (6.0-7.5‰) and radiogenic Hf isotopes (ε_{Hf} = +3 to +4) in rocks of ~1.2 Ga age. Together, these age and isotopic data indicate the presence in cratonic East Antarctica of a large, composite igneous province that formed through a punctuated sequence of relatively juvenile Proterozoic magmatic events. Further, they provide direct support for geological correlation of crust in East Antarctica with both the Gawler Craton of present-day Australia and Proterozoic provinces in western Laurentia. Prominent clast ages of ~2.0, 1.85, 1.57 and 1.45 Ga, together with sediment source linkages, provide evidence for the temporal and spatial association of these cratonic elements in the Columbia supercontinent. Abundant ~1.2-1.1 Ga igneous and metamorphic clasts may sample crust underlying the Gamburtsev Subglacial Mountains, indicating the presence of a Mesoproterozoic orogenic belt in the interior of East Antarctica that formed during final assembly of Rodinia.

Key words: igneous rocks, granitoids, East Antarctica, U-Pb geochronology, O and Hf isotopes

INTRODUCTION

The nature of Antarctic continental lithosphere is Earth's last geological frontier. The Precambrian cratonic elements of the East Antarctic shield are of similar size as Australia or the contiguous U.S., yet, because of extensive ice cover and sparse remote-sensing data, this composite shield remains largely unexplored except for locally well-known coastal geological exposures (Harley and Kelly, 2007). Further, there is virtually no basement outcrop for about a third of its perimeter along the Transantarctic Mountains (TAM) margin, which are underlain mainly by Phanerozoic rock assemblages. Despite large gaps in our understanding, however, the East Antarctic lithosphere is globally important because: (1) as one of the largest coherent Precambrian shields, including rocks as old as ~3.8 Ga, it represents an important component in the global crustal growth history (Condie and Aster, 2010; Hawkesworth et al., 2016); (2) it is a key piece in assembly of the Columbia (~2 Ga), Rodinia (~1 Ga) and Gondwana (0.6-0.5 Ga) supercontinents (e.g., Fitzsimons 2003; Boger 2011; Ferraccioli et al., 2011; Harley et al. 2013; Goodge and Fanning, 2016), the assembly and breakup of which are associated with major changes in paleogeographic, sediment dispersal, geochemical, and biotic patterns (e.g., Lindsay and Brasier, 2002; Moores, 2002; Nance et al., 2014; Gernon et al., 2016); (3) it is the substrate to Earth's largest ice cap (East Antarctic ice sheet), including numerous subglacial lakes, and influences its thermal state and mechanical stability (Pollard et al., 2005; Jamieson and Sugden, 2008; Van Liefferinge and Pattyn, 2013; Schroeder et al., 2014); and (4) its geotectonic association with formerly adjacent cratons in South Africa, India and Australia suggests that it might harbor important mineral resources. Despite the influence of the East Antarctic shield on these processes and events, however, there is scant direct evidence concerning its age, composition, internal structure, and petrogenesis.

Uncovering the ice-covered geology of East Antarctica is therefore critical for understanding its ancient crustal history, its role in supercontinent formation, and its relationship to development of the Cenozoic ice cap. For example, despite seismological evidence for thick, cold lithosphere across much of East Antarctica (e.g., An et al., 2015), we have little explicit knowledge about its age and composition

except from limited coastal and mountain rock exposures. Likewise, hypotheses for crustal provinces and boundaries related to assembly of the East Antarctic shield (e.g., Fitzsimons, 2003; Boger, 2011) are based mainly on extrapolation of coastal geology toward the interior, yet these models are largely unconstrained very far inland. Also, ideas concerning the origin and evolution of the completely buried Gamburtsev Subglacial Mountains, some including hypotheses of orogenic activity (e.g., Ferraccioli et al., 2011), are permissive based on interpretation of potential-field geophysical data but lack direct evidence of geologic age and composition. Despite the ambiguities inherent in studying a continent covered by a thick ice sheet, it is clear that multiple approaches—including detrital-mineral provenance study, analysis of glacial clasts, airborne and ground-based geophysics, and future sub-glacial drilling—are improving our view of the remote continental interior. Proxy geologic materials such as detrital zircons and glacial clasts provide a means to sample the ice-covered crust, although spatial-geographic resolution is poor; conversely, geophysical data are spatially precise yet limited by uncertainty in geologic interpretation. In addition to U-Pb zircon ages of ~3.1, 2.5 and 1.7 Ga from outcrops of the Nimrod Complex (e.g., Goodge and Fanning, 2016), an isolated basement assemblage adjacent to central East Antarctica, detrital-zircon provenance and glacial clast studies from the central Transantarctic Mountains show that the continental interior was formed by a series of episodic magmatic events between about 2.0-1.1 Ga (Goodge et al., 2004, 2008, 2010). Whereas geophysical data provide insight into lithospheric properties and internal structure (e.g., Aitken et al., 2014; An et al., 2015), and the geology circumscribing East Antarctica provides specific age constraints that outline a long-lived Mesoarchean to Mesoproterozoic history (Harley and Kelly, 2007; Harley et al., 2013), much can be gained from rock samples recovered from the continental interior.

Our main goal in this study is to illuminate the geology of the ice-covered East Antarctic shield, document its crustal history, and evaluate correlations with other cratons in order to test and develop supercontinent growth models. The approach we adopted is to sample igneous and metamorphic rock clasts from glacial moraines sourced within central East Antarctica (Fig. 1). Our focus is on analysis of

accessory minerals such as zircon to determine their U-Pb ages, and Hf and O isotopic compositions. Because of its robust nature and host to different trace elements, zircon is a rich repository of age and isotopic information that can be used to assess crustal composition and process as a function of time (Hawkesworth and Kemp, 2006; Kemp et al., 2006; Harley and Kelly, 2007; Scherer et al., 2007; Condie et al., 2009). Zircons are abundant in many rock types, often occur as composite grains with complex internal structure, contain valuable isotopic and trace-element information, are refractory and resistant to high-*T* chemical change, and provide arguably the best geochronometer available (via the U-Pb system) to address a wide range of geological processes. Long used as an age tool, continuing advances in analytical approaches (in particular: SIMS; LA-MC-ICPMS; and LASS[1]) allow for the *in situ* measurement of many elements and isotopes, making it possible to associate age and isotopic tracer information to specific growth stages and conditions. A focus in this study on zircon from glacial igneous rock clasts can therefore provide critical data about age and inheritance (U-Pb), the involvement of hydrated crustal or mantle source materials (O isotopes), and mantle vs. crustal sources during their evolution (Hf isotopes). Together with whole-rock geochemical analyses, new zircon age and isotopic data can help to refine models of crustal assembly in East Antarctica, provide constraints on models of Columbia and Rodinia supercontinent assembly, provide new details of the cratonic substrate to the East Antarctic ice sheet, and help guide future subglacial bedrock coring in the interior of East Antarctica.

Because so little of the Precambrian shield of East Antarctica is exposed in either the Transantarctic Mountains or coastal areas, bedrock erosion by glacial flow can provide natural proxy samples of the continental interior (e.g., Peucat et al., 2002; Goodge et al., 2008, 2010). Major ice streams in East Antarctica are marked by nearly radial flow away from central ice divides and domes toward the continental margin (Fig. 1a). Unique among the major ice-stream systems, glacial ice in the Byrd Glacier and related smaller drainages moves laterally from the main ice divides and is obstructed by the high-standing Transantarctic Mountains (peak elevations >4000 m). Ice flows through the mountains via

[1] SIMS, secondary-ion mass spectroscopy; LA-MC-ICPMS, laser-ablation multi-collector inductively-coupled plasma mass spectroscopy; LASS, laser-ablation split stream.

channelized outlet glaciers, but it also ablates in areas where it ramps up against the mountain range (Whillans and Cassidy, 1983). Glacial moraines are formed both along the margins of the outlet glaciers and where ice is ablating, forming lag deposits adjacent to the mountains. For this study, we targeted about a dozen sites extending >1500 km along the length of the Transantarctic Mountains where glacial moraines are exposed, from the Convoy Range in southern Victoria Land to Strickland Nunatak near Reedy Glacier (Fig. 2). Ice velocity fields show that material transported in the greater Byrd Glacier system may have been eroded from a broad area of central East Antarctica, potentially from near the upstream boundary along the major ice divide connecting Dome A and Dome C (Fig. 1).

This study reports findings from geochemical, geochronological, and isotopic analysis of a subset of igneous rock clasts collected from glacial deposits flanking the Transantarctic Mountains. The rocks considered here consist mainly of intermediate to felsic igneous rocks, mostly of granitoid composition, representing magmatic components of the ice-covered East Antarctic craton. Many of the samples are meta-igneous rocks with deformation fabrics and/or metamorphic mineralogies that reflect a multi-stage history of initial crystallization and overprinting. Here we report new whole-rock major- and trace-element compositions, U-Pb zircon ages, and O- and Hf-isotopic compositions for a suite of 22 igneous clasts. Populations with ages between about 2.0-1.0 Ga provide new constraints on the Proterozoic crustal history of central East Antarctica, including magma sources, crustal inheritance, and periods of deformation. Age and isotopic correlations between these samples and rocks in both Australia and Laurentia strengthen paleogeographic ties during the Proterozoic assembly of the supercontinents Columbia (or Nuna; see Meert, 2012) and Rodinia.

APPROACH AND ANALYTICAL METHODS

This study focused on five sites in the general area of the Byrd Glacier drainage—Argo Glacier, Lonewolf Nunataks, Milan Ridge, Mt. Sirius, and Turret Nunatak—that yielded pre-Ross igneous clasts, thereby providing evidence regarding composition and age of the Precambrian East Antarctic shield (Figs.

1 and 2; Table 1). One of the most productive sites at Lonewolf Nunataks consists of elongate bands of distributed moraine and ice-matrix debris along narrow flow lines related to ice movement along the southern margin of Byrd Glacier (Fig. 3a). Sites at Milan Ridge and Argo Glacier, directly adjacent to exposed Precambrian basement in the Miller Range, comprise thin, distributed morainal deposits dominated by a rich variety of crystalline rock types. Sites at Turret Nunatak and Mt. Sirius are dominated by clasts of Jurassic Ferrar-type tholeiitic dolerites or sedimentary rocks of the Beacon Supergroup (Devonian to Triassic Gondwana strata), but they also yielded a small number of distinctive crystalline clasts described here. Brief sample descriptions, photographs of the analyzed clasts, photomicrographs in thin section, and representative images of zircons are provided in Appendix 1. The mineralogy of the analyzed clasts is listed in Supplementary Data Table 1.

Prospective sample sites were identified from topographic maps, aerial photographs, and satellite imagery where visible morainal deposits appeared to have been sourced from the continental interior. Sample sites, including large composite moraine complexes, small isolated moraines, and glacier-margin deposits, were visited by Twin Otter aircraft and helicopter. Materials at sites we sampled consisted of heterolithic boulders to cobbles, unsorted grain material down to sand size, and fine silt. Small boulders and cobbles collected for this study typically have round, subequant shape, with smooth surfaces and visible striations (Fig. 3b). At each sample site, we covered as large an area as possible given our allotted ground time and collected all rock clasts that showed potential for geochronology and study for either their igneous or metamorphic petrology. At many sites, boulder and cobble material was dominated by Ferrar dolerites or Beacon sedimentary rocks, which are exposed principally at relatively higher elevations of the Transantarctic Mountains; because these rocks post-date the Ross Orogeny and have a local source unrelated to the cratonic interior, they were not sampled. Virtually any other crystalline rock was collected, thus providing a qualitatively randomized sample set. While at the sites, whole collections were then subdivided into different petrographic groups based on color, mineralogy, and texture, and catalogued by name and a brief description.

Our search for samples showing Precambrian ancestry in the East Antarctic shield was complicated by the widespread and pronounced thermomechanical effects of the Ross Orogeny, rendering it impossible to determine from petrographic inspection alone whether a given rock clast sampled from glacial moraines adjacent to the Transantarctic Mountains had a Ross or pre-Ross origin. For this reason, a thorough and careful process was undertaken to maximize our chances of success in finding examples of pre-Ross crystalline basement. We adopted a step-wise procedure beginning with initial petrographic study, followed by *in situ* reconnaissance U-Pb zircon geochronology, full mineral separation, and finally the preparation of zircon grain mounts for detailed age and isotopic analysis. From a field collection of >300 individual rock samples, our strategy for prioritizing a small subset of samples for analysis began by giving highest initial priority to clast samples that represented as broad a spectrum as possible of mineralogy, composition, and texture and which also were of large enough size to yield sufficient zircon mineral separates. After assigning priority based on gross hand-sample characteristics, further ranking of the igneous samples was based on petrographic characteristics, including confirmation that the sample contained accessory zircon. From the entire collection, we culled a group of 40 samples for geochemical, age, and isotopic analysis.

Once a set of sample candidates was defined, polished thin sections were analyzed at Washington State University for *in situ* reconnaissance U-Pb geochronology by LA-ICPMS. Mapped zircons were located and analyzed using a New Wave UP-213 laser ablation system coupled to a single collector ThermoFinnigan Element2 mass spectrometer. Samples giving Ross Orogen-type zircon U-Pb ages (~500 Ma) were not considered for further analysis, leaving a subset of 22 samples with older U-Pb ages reflecting a Precambrian crustal ancestry that became the focus of all subsequent detailed age and isotopic analysis. For analysis of this final sample set, we adopted the following general analytical sequence for each sample (detailed methods explained in Appendix 2). First, zircons were separated using standard crushing and heavy liquid techniques, and polished zircon-grain epoxy mounts were prepared at the Australian National University. Transmitted-light and cathodoluminescence (CL) images of the zircon

populations were acquired for all samples and used as the basis for selecting spots for age analysis. U-Pb ages were determined by Sensitive High-Resolution Ion MicroProbe (SHRIMP) analysis at the ANU. After light polishing to remove the U-Pb pits and re-coating, O-isotope compositions were analyzed by SHRIMP II on the same areas used for U-Pb isotope analysis in order to assign an O isotopic composition to a particular age domain. Sample mounts were then analyzed for their Hf-isotope compositions using the ThermoFinnigan Neptune MC-LA-ICPMS instrument at Washington State University, again by superimposing laser spots on the same spots used for SHRIMP analysis. Following this sequence, we were able to characterize the age and O- and Hf-isotope compositions of zircons, providing correlated age, stable isotope and radiogenic isotope information for each sample. Detailed analytical procedures are given in Appendix 2.

Bulk-rock XRF and ICPMS analyses of major and trace element compositions for most of the dated samples were completed at Washington State University. Detailed analytical procedures are given in Appendix 2.

RESULTS

Geochemical compositions

Major, trace and rare-earth element geochemical data for the granitoid clasts are listed in Supplementary Data Table 2. All samples are Si-rich with >65 wt% SiO_2, and many have SiO_2 = 70-75 wt%. Petrographically, some samples are two-mica granitoids and all are peraluminous in composition with Al/(Ca-1.67P+Na+K)>1. As a group, these granitoids are generally magnesian rather than ferroan, based on Fe/Mg trends relative to Si (Fig. 4a; Frost et al., 2001), and they range mainly from alkali-calcic to calc-alkaline compositions (Fig. 4b). A number of samples show a high degree of alteration, indicated by the presence of chlorite, sericite, epidote, calcite and other minerals (see Supplementary Data Table 1), such that major-element geochemical compositions may have been modified since initial igneous

crystallization. Trace-element spider diagrams show that the samples have enriched LREE and depleted HREE abundances relative to chondrites (Fig. 5a), and they are enriched in LIL elements and slightly depleted in HFS elements relative to MORB (Fig. 5b).

U-Pb geochronology

Of the 40 samples analyzed in reconnaissance, 22 yielded pre-Ross Orogen ages that can be divided into six different age groups on the basis of their SHRIMP U-Pb dates (Table 1). A brief summary of the age results is provided here, primarily to identify the principal igneous crystallization ages and constrain the ages of any evident younger metamorphism or deformation. Wetherill-type concordia diagrams and age probability distributions for each set of sample analyses are shown in Figures 6-11. Complete age data from individual samples are listed in Supplementary Data Tables 3-24 and a detailed presentation of U-Pb age results for each sample, including zircon characteristics and brief petrographic descriptions, is provided in Appendix 3. A summary of sample mineralogy is listed in Supplementary Data Table 1 and representative images of the samples and zircons are provided in Appendix 1.

Group 1 (1205-1220 Ma). Two granitoids from Lonewolf Nunataks yielded ages of ca. 1205-1220 Ma (Fig. 6). Sample 10LWA-13.1 is an undeformed muscovite-biotite granite. Zircons from this sample show dominantly zoned igneous features, either length-parallel zoning or sector zoning in the more equant grains. An array of concordant analyses was deconvolved using a mixture modeling algorithm (Sambridge and Compston, 1994) in order to identify the dominant grouping with a $^{207}Pb/^{206}Pb$ age of 1204 ± 12 Ma (Fig. 6a). A weighted mean $^{207}Pb/^{206}Pb$ age for 10 analyses also gives 1204 ± 12 Ma (MSWD = 0.93). Interpretation of this age as reflecting crystallization rather than Pb loss is further supported by Hf-isotope compositions of the individual grains (see Hf-isotope section, below). A second sample (10LWA-11.1) is a biotite granite that shows evidence of recent Pb loss but which yielded an upper intercept age at 1218 ± 15 Ma and a weighted mean $^{207}Pb/^{206}Pb$ age of 1213 ± 14 Ma (Fig. 6b), which provides the best estimate for igneous crystallization of this rock.

Group 2 (1410-1505 Ma). Ten red- to grey-colored granitoids collected from four sites yielded ages of ca. 1410-1505 Ma (Figs. 7a-7j). They are similar in character and age to samples collected previously from Turret and Lonewolf nunataks, with ages of 1441 ± 6 and 1459 ± 6, respectively (Goodge et al., 2008, 2010). Most of the new samples show relatively simple U-Pb behavior, yielding either concordia, upper-intercept, or weighted-mean $^{207}Pb/^{206}Pb$ ages that provide robust estimates of crystallization age. One sample (10TNA-1.1) has a distinctive rapakivi-type, porphyritic texture and yielded a concordia age of 1430 ± 16 Ma (Fig. 7c). Several samples from this group have deformation fabrics, and two (10LWB-4.3 and 10LWA-9.2) have precise zircon ages that constrain the timing of deformation to less than ~1450 Ma.

Three samples show U-Pb evidence of Grenville-age overprinting. Sample 10MSA-2.3 (1410 ± 10 Ma) yielded a prominent tight grouping of near to concordant analyses (Fig. 7a), with other dispersed analyses trailing down the concordia curve towards 1150 Ma, likely reflecting radiogenic Pb loss during a Grenville-age event. Sample 10LWA-6.6 is a foliated muscovite-biotite granite that yielded an upper intercept age of 1452 ± 6 Ma (Fig. 7e); one grain with low Th/U = 0.06 and large isotopic uncertainties gives an apparent $^{206}Pb/^{238}U$ age of ~1200 Ma, which may reflect post-crystallization alteration or metamorphism. Sample 10MSA-3.5 (1506 ± 11 Ma) is a foliated muscovite-biotite leucogranite showing evidence of multi-stage radiogenic Pb loss (Fig. 7j). Some zircons in this sample have narrow unzoned secondary rims that all yield Grenvillian $^{207}Pb/^{206}Pb$ dates. We suggest that the primary igneous zircon crystallization occurred around 1500 Ma with a second zircon crystallization event at about 1200 Ma. Thus, three samples of Mesoproterozoic granitoids show evidence of subsequent metamorphism between about 1200-1150 Ma.

Group 3 (ca. 1570 Ma). One granitoid collected at Lonewolf Nunataks yielded a distinctive age of ca. 1570 Ma (Fig. 8). Sample 10LWA-6.4 is a foliated muscovite-biotite granite. Most of the zircons in this sample are metamict, but the dominant concordant analyses can be fitted with a regression giving an upper-intercept age of 1569 ± 10 Ma. Three other analyses track down Concordia, likely indicating some

radiogenic Pb loss during a Grenvillian event as seen in Group 2. There are also some altered and inherited older components (see Supplementary Data Table 15). Analyses from oscillatory-zoned rims yielded a weighted-mean $^{207}Pb/^{206}Pb$ age of 1570 ± 10 Ma that we interpret to constrain the time of igneous zircon crystallization.

Group 4 (1785-1800 Ma). Two granitoids from two different sites at Lonewolf Nunataks and Milan Ridge yielded ages of ca. 1785-1800 Ma (Fig. 9). Sample 10LWA-14.1 is a biotite granite marked by extensive alteration, veins and fractures. Zircon analyses in this sample form a discordia trend with an upper intercept at 1820 ± 22 and lower intercept of ~1130 Ma (Fig. 9a). However, due to multiple radiogenic Pb loss effects, a more reasonable estimate of zircon crystallization is given by a weighted-mean $^{207}Pb/^{206}Pb$ age of 1786 ± 8 Ma for the analyses that constrain the upper concordia intercept. We consider this age to be the best estimate for igneous crystallization, although based on its texture and lower-intercept age this rock has experienced significant Grenville-age alteration and brecciation.

Sample 10MRA-2.1 is a garnet-biotite granite orthogneiss displaying a weak foliation and microtextures indicating post-magmatic recrystallization. Zircons in this sample form two general groupings or clusters on a Wetherill concordia plot, with Mesoproterozoic (~1200 Ma) and Paleoproterozoic (~1780 Ma) ages (Fig. 9b). The older grouping comprises two distinct subgroups, with respective concordia upper-intercepts at 1798 ± 17 Ma and 1785 ± 23 Ma. We regard the older age as providing a constraint on the primary igneous crystallization of this rock, and the slightly younger age represents either a second period of zircon crystallization or was caused by radiogenic Pb loss. Five younger grains or rims yielded nearly-concordant $^{207}Pb/^{206}Pb$ ages of about ~1190 Ma, likely reflecting a partial melting event during Grenvillian time.

Group 5 (1850-1875 Ma). Five granitoids from three different sites yielded ages of ca. 1850-1875 Ma (Fig. 10). A granite with a similar age of 1878 ± 7 Ma was also reported from Lonewolf Nunataks by Goodge et al. (2010). All five samples give well-defined U-Pb concordia, weighted-mean, or upper-intercept ages, and four have deformation fabrics that formed during or after crystallization. Three of the

samples in this group show zircon U-Pb evidence of Grenville-age overprinting, including a lower intercept age of ~1185 Ma (10LWA-6.3), a lower intercept at ~1140 Ma (10LWB-4.1), and seven rim analyses with Th/U ratios between 0.29-0.99 that are consistent with a magmatic paragenesis yet yield a weighted-mean $^{207}Pb/^{206}Pb$ age of 1166 ± 11 Ma (10MSA-3.3). Together, overgrowth ages of ~1185, ~1140 and ~1165 Ma from samples in this group provide firm evidence that these Paleoproterozoic igneous rocks experienced Grenvillian metamorphism and deformation.

Group 6 (2010-2015 Ma). Two granitoids collected at Lonewolf Nunataks yielded ages of ca. 2010-2015 Ma (Fig. 11). Sample 10LWA-10.1 is weakly-foliated hornblende-biotite granite with a weighted-mean $^{207}Pb/^{206}Pb$ magmatic crystallization age of 2010 ± 3 Ma (Fig. 11a). Sample 10LWA-8.1 is a foliated garnet-hornblende-biotite orthogneiss; the zircon analyses form a discordant array to which a best-fit regression gives an upper-intercept age of 2015 ± 12 Ma (Fig. 11b), which we regard as the best estimate for magmatic crystallization of this rock.

Age summary. A histogram and relative probability distribution of the U-Pb ages reported here, including previously reported age data for eight clasts from Goodge et al. (2008, 2010), shows at least six discrete age populations (Fig. 12). Importantly, the reproducibility evident from multiple samples in each age group shows that these are not merely random crustal samples, but rather that the glacial ice streams have eroded discrete geological units or provinces. Interestingly, the age populations identified here do not match any of the known basement ages reported for crystalline bedrock exposed in the Transantarctic Mountains, past which these ice streams flow (principal igneous and metamorphic ages of about 3.1, 2.5, and 1.7 Ga; see Goodge and Fanning, 2016). Therefore, these glacial clast ages appear to have sampled previously unknown Paleoproterozoic and Mesoproterozoic magmatic crust of East Antarctica. In addition, two samples from Group 1 with magmatic crystallization ages of ca. 1220-1205 Ma, and eight other samples showing evidence of either new igneous or metamorphic zircon crystallization between 1200-1130 Ma, demonstrate the presence of either a prominent Grenville-age crystalline terrain or a widespread Grenvillian overprint in the source region.

O-isotope compositions

Zircon O-isotope compositions are listed in Table 2 and plotted by age group in Figure 13. Complete O-isotope analyses are listed in Supplementary Data Table 25. The average compositions reported here typically have a 2σ external uncertainty of about 0.5 per mil. The compositions of two Group 1 samples (1120-1205 Ma) do not overlap (7.4 and 5.8 ‰) and show mixed crustal and mantle-like $\delta^{18}O$ signatures. Most of the Group 2 samples (1505-1410 Ma) have low, mantle-like $\delta^{18}O$ signatures (~4-5 ‰), but two have compositions >7 per mil that indicate incorporation of pre-existing crustal sources; the samples with low $\delta^{18}O$ might also reflect alteration in the presence of meteoric water. Samples from groups 3, 4 and 5 (ca. 1570, 1790 and 1850 Ma) have mostly crustal $\delta^{18}O$ compositions >6 per mil. One sample from Group 4 (10MRA-2.1) has an unusually low $\delta^{18}O$ composition of 3.8 ± 0.4 per mil that may indicate alteration in the presence of meteoric water. Two samples from Group 6 have consistent mantle-like $\delta^{18}O$ signatures of about 4.0 to 4.5 per mil.

Low $\delta^{18}O$ values (3-5 per mil) can arise from any of the following: (1) the analysis of flawed crystal areas; (2) post-crystallization deuteric alteration of the areas analyzed, particularly by ice and/or water during transport of these glacial clasts; or (3) crystallization of zircon from a source that was itself hydrothermally altered prior to melting. In one case (e.g., 10MRA-2.1), both transmitted light and CL images show that the zircons in this sample have abundant cracks, opaque areas, and complicated CL patterns indicative of post-crystallization alteration. The consistency of individual spot analyses within most samples, and the similarity of values for multiple samples in both the 1450 and 2010 Ma groups suggests, however, that the low values in these groups are real and therefore likely due to pre-magmatic alteration in the source region.

Hf-isotope compositions

The Hf isotope data for zircons in each sample are presented as the weighted mean of multiple laser analyses (based on 6-15 analyses per sample; Table 3). For individual samples, the total variance within a population of measurements was typically small (2SD = 2 ε_{Hf} units or less; see complete Hf-isotope data listed in Supplementary Data Table 26), indicating a single isotope composition for each sample. Thus, we present the initial ε_{Hf} data for each sample as a single weighted mean. Both individual spot and mean compositions are plotted by age group in Figure 14a. The two samples from Group 1 (1205-1220 Ma) have initial ε_{Hf} values of +3 and +4. Seven samples from Group 2 (1410-1505 Ma) have initial ε_{Hf} values ranging from +7 to +10, and two overlap with the depleted-mantle evolution. A single sample from Group 3 (ca. 1570 Ma) has a lower initial ε_{Hf} (-3) compared to the younger age groups. Six of the seven samples from Groups 4 (1785-1800 Ma) and 5 (1850-1875 Ma) have unradiogenic Hf (ε_{Hf} values from about -1 to -6) with a single sample having considerably more radiogenic Hf (ε_{Hf} = +5). The two Group 6 (2010-2015 Ma) samples have initial ε_{Hf} of about +1.5. Zircon depleted-mantle Hf model ages (T_{DM}) are listed in Table 3.

Hf-isotope compositions can be effectively used to evaluate Pb-loss behavior in U-Pb zircon ages, as conditions leading to Pb loss are not expected to modify the $^{176}Hf/^{177}Hf$ composition, while growth of new zircon at a later date would inherit the $^{176}Hf/^{177}Hf$ of fluid or melt from which it was grown (e.g., Amelin et al., 2000; Gerdes and Zeh, 2009). A number of samples show normal Pb-loss behavior related to post-crystallization geological events (e.g., 10LWA-11.1; Fig. 6b). However, sample 10LWA-13.1 from Group 1 (Fig. 6a) shows a spread of analyses along Concordia that is more difficult to interpret. In this case, a deconvolution algorithm was applied in order to identify the best estimate for crystallization of ca. 1204 Ma. Six analyses from this sample, however, yield homogeneous $^{176}Hf/^{177}Hf$ over a range of $^{207}Pb/^{206}Pb$ ages, consistent with a history of Pb loss. Similarly, for sample 10MSA-3.5 from Group 2 (1506 Ma; Fig. 7j), a comparison of measured initial $^{176}Hf/^{177}Hf$ ratios vs. $^{207}Pb/^{206}Pb$ age shows that all grains have similar $^{176}Hf/^{177}Hf$, supporting the interpretation for Grenville-age Pb-loss.

DISCUSSION

Geochemical patterns

Because these samples are of different ages and unknown geological association, we do not expect patterns or trends to emerge from their geochemical compositions. However, they exhibit some general similarities that indicate a common magmatic origin. As a group, the samples show decoupled LIL/HFS ratios and a Ta-Nb 'trough' that is typical of subduction-zone melts. Most samples show a negative Eu anomaly, indicating that plagioclase was a strongly fractioning early phenocryst phase during crystallization. Thus, their trace and rare-earth element signatures are quite similar to modern continental-margin magmatic arc systems (e.g., Cascades, Andes) or evolved volcanic arcs, and they show very similar patterns and abundances as magmas interacting with thick crust (e.g., Davidson et al., 1990, 1991; Wörner et al., 1994). Some of the samples resemble Si-rich, peraluminous leucogranites found in regions of over-thickened continental crust (Frost et al., 2001). In broad terms, the trace-element compositions indicate that the melts that produced these igneous rocks interacted with thick, evolved continental crust, but that they are dissimilar generally from intraplate granitoids.

Tectonic discrimination diagrams also show affinity with volcanic-arc granitoids, although some have similarities to within-plate types (Figs. 4c, 4d; Pearce et al., 1984). In several respects, they show Mg-enrichment and calc-alkaline to calcic trends typical of Cordilleran-type granites found in continental-margin magmatic settings (Frost et al., 2001), although the 2010 Ma samples (Group 6) are notably more calcic and depleted in Rb compared to the other groups.

Granitoids of ca. 1450 Ma age (Group 2) are similar in age to a prominent belt of Mesoproterozoic granites in Laurentia that are commonly referred to as A-type or anorogenic granites (Anderson, 1983; Anderson and Bender, 1989). The Laurentian granitoids of this age have melt sources mainly in pre-existing Paleoproterozoic crust (Anderson and Morrison, 2005; Goodge and Vervoort, 2006). Based on textural, mineralogical, geochemical, age, and isotopic characteristics, igneous clasts with similar age from Turret Nunatak and Lonewolf Nunataks were previously suggested to represent an Antarctic

extension of this distinctive Laurentian belt into East Antarctica (Goodge et al., 2008, 2010). Some of our new samples from Group 2 are notably more magnesian and less alkalic than most traditionally defined A-type, or ferroan, granites (Fig. 4a), and they should not be considered as strictly A-type or ferroan in composition (Frost and Frost, 2011). However, most of the 1450 Ma group of clasts show SiO_2 and FeO* compositions that overlap with the peraluminous two-mica and, to a lesser extent, magnetite-series groups of Mesoproterozoic granitoids found in Laurentia (Fig. 4a; Anderson and Cullers, 1999; Anderson and Morrison, 2005), indicating a geochemical affinity.

Age and source relations

The age distribution demonstrated from U-Pb analysis of igneous glacial clasts sourced in central East Antarctica shows a heretofore unrecognized and episodic Proterozoic growth of continental East Antarctica between 2.0 and 1.0 Ga (Fig. 12). This age distribution is not currently known from geological exposure and provides a unique encapsulation of crustal history in the broader ice-covered shield.

The two samples from the oldest group in this study (Group 6, ~2010 Ma) have both overlapping age and initial ε_{Hf} values, indicating a close petrogenetic relationship between these two glacial clasts. Zircons from Group 6 have both mantle-like $\delta^{18}O$ signatures, near-chondritic Hf-isotope compositions, and depleted-mantle model ages of ~2.3 Ga. Their initial ε_{Hf} value of about +1.5 indicates incorporation of some pre-existing crust during this magmatic event (Fig. 14b), but whether they have a simple history evolved from older crust or represent a mixture of older crust and younger, juvenile melts is not clear from just two samples. Most of the seven samples comprising Groups 4 and 5 (composite age range of about 1875-1785 Ma) have O-isotope compositions indicating derivation from pre-existing crustal sources, yet they have a large range in initial ε_{Hf} values (-7 to +5). Depleted-mantle model ages range from about 2.0-2.5 Ga. About a third of the samples come from this composite group (7 of 22), suggesting that 1875-1785 Ma was a period of prolific magmatism, while their large range of initial ε_{Hf} from both positive to negative values demonstrates that this was a period (~1.85 Ga) of both new crustal additions as well as assimilation by reworking of older, more evolved crust (Fig. 14b). This period of

crustal growth has been recognized globally (e.g., Iizuka et al., 2005; Condie and Aster, 2010). The least radiogenic samples in this composite group have initial ε_{Hf} values that are too negative to be explained by derivation solely from Group 6, and require more evolved crust than was sampled during this investigation. Depleted-mantle model ages of ~2.5 Ga for these least radiogenic samples indicate the influence of pre-existing Neoarchean crust (Fig. 14b), which has also been recognized as a period of significant crustal addition worldwide (e.g., Condie and Aster, 2010). The single sample from Group 3 (ca. 1570 Ma) has a crustal $\delta^{18}O$ value (8.1 ‰) and a moderately evolved initial ε_{Hf} composition of -3 and T_{DM} age of ~2.2 Ga; assuming a simple isotopic evolution, it appears to have formed in part by incorporation of some pre-existing Paleoproterozoic crust. Nearly half of the samples in our study (10 of 22) range in age from about 1410 to 1505 Ma (Group 2), suggesting that this also was an important period of magmatic activity. However, their isotopic compositions reflect a significantly different petrogenetic history. In addition to low, mantle-like $\delta^{18}O$ values, zircons from Group 2 also have radiogenic Hf-isotope signatures indicating derivation from a depleted mantle source with little, if any, input of older crustal material. Depleted-mantle model ages for this group are consistently in the range of about 1.5-1.6 Ga. Notably, the oldest samples from this group are the most juvenile found in this study, having initial ε_{Hf} values of about +10 (Fig. 14b), in close agreement with the depleted mantle model proposed by Vervoort et al. (2015) and demonstrating that ~1.5 Ga was a time of significant crustal growth, as has been suggested for the so-called A-type magmatic province of North America (e.g., Anderson and Bender, 1989; Van Schmus et al., 1993; Anderson and Morrison, 2005; Goodge and Vervoort, 2006). The five younger (i.e., <1470 Ma) samples in this group have slightly more evolved ε_{Hf} values (+6.6 to +8.2) than the older ones; this can be explained by derivation of the younger samples in Group 2 entirely from crust represented by the older samples in this group. Alternatively, these slightly more evolved values in the younger samples may indicate incorporation of some minor portion of even older pre-existing crust. This interpretation is consistent with elevated $\delta^{18}O$ in two of the samples (about +7 to +8; Fig. 13), which indicates that these melts were in chemical communication with older crust. Finally, the two youngest samples in this study (Group 1, ~1210 Ma) have similar ages, $\delta^{18}O$ values indicating derivation from pre-

existing crustal sources, ε_{Hf} values (about +3 to +4), and T_{DM} ages of about 1.6 Ga. Assuming the source region of Group 2 evolved with a typical crustal $^{176}Lu/^{177}Hf$ ratio of 0.0125, the origin of Group 1 can best be explained by derivation from a source region comprised mainly of Group 2 granitoids ~250 m.y. after the proposed ~1.5 Ga crustal growth event.

Analysis of zircon Hf and O isotope compositions with respect to age (Fig. 15) can help to distinguish the relative roles of crustal and mantle contributions to the magmas. The oldest samples (Group 6, ~2010 Ma) have initial ε_{Hf} values consistent with incorporation of pre-existing Paleoproterozoic crust, but their evolution appears distinct from other groups in the whole suite (Fig. 14b) and their $\delta^{18}O$ compositions are about 1 per mil lower than typical mantle values, indicating alteration in the presence of meteoric water. Collectively, groups 3, 4 and 5 have mostly positive $\delta^{18}O$ and negative ε_{Hf} values indicating involvement of, or interaction with, evolved, pre-existing crust. One of the samples from Group 4 has a low $\delta^{18}O$ composition that probably reflects post-magmatic secondary alteration not observed in the other sample from this group. The older group 4 and 5 samples, with ages of ~1850 and ~1790 Ma, respectively, appear to indicate derivation from Neoarchean to oldest Paleoproterozoic crust, whereas the ~1570 Ma sample (Group 3) indicates derivation from a younger crustal source. In contrast to the older samples, the Mesoproterozoic samples have a much more juvenile, mantle-derived signature. In particular, Group 2, with ages of ~1450 Ma, have low $\delta^{18}O$ compositions and strongly positive radiogenic ε_{Hf} compositions, indicative of a primary mantle melt origin. Group 1 samples (~1210 Ma) have $\delta^{18}O$ compositions reflecting an origin as crustal melts; their less radiogenic Hf isotope compositions (slightly positive ε_{Hf} values) are consistent with melting of pre-existing ~1.45 Ga crust (represented by Group 2).

In summary of their petrogenetic and crustal history, the zircon U-Pb ages of these igneous glacial clasts—together with their O- and Hf-isotopic compositions—allow us to conclude the following: (1) the discrete ages and, in some cases, consistent isotopic compositions within age groups indicate that samples in most groups are genetically related and not merely of coincidentally similar age, providing evidence that the glacially-derived clasts are samples of geologically distinct sub-glacial rock assemblages; (2)

samples from Groups 2, 4 and 5 make up the majority of this sample suite (17 of 22), from which we infer that magmatic events at ca. 1.45, 1.79 and 1.86 Ga are important in the growth of East Antarctica; (3) Hf-isotope compositions indicate that the older samples in Groups 4, 5 and 6 (2.0-1.8 Ga) were derived primarily from pre-existing crust formed between about 2.7-2.1 Ga; (4) the range in initial ε_{Hf} among samples in the older groups (-7 to +5) further indicates that they formed as melts involving mixtures of different sources, perhaps a mixture of juvenile components with contributions from older, pre-existing crust (e.g., Group 5, ca. 1.85 Ga); (5) melts formed at about 1.45 Ga (Group 2) have juvenile, mantle-like O- and Hf-isotope compositions; and (6) melts formed at about 1.21 Ga appear to have been derived primarily from pre-existing crust and are consistent with re-melting of 1.45 Ga sources.

Implications for East Antarctic shield history

The new data reported here add significant detail to the distribution of crustal domains inferred to underlie the ice cap adjacent to the central Transantarctic Mountains (Goodge et al., 2008, 2010). As shown in Figure 16, the new ages identified at five glacial moraine sites define a region of Proterozoic igneous crust comprised by discrete age populations (Groups 1-6). Crystalline igneous and metamorphic basement rocks of the Nimrod Complex exposed in the nearby Miller and Geologists ranges record a distinctly different history, including major events at ca. 3.1, 2.5 and 1.7 Ga (Goodge and Fanning, 2016). There is no overlap in ages between the glacial clasts and the exposed basement. This distinction led Goodge et al. (2010) to define a crustal domain referred to as the Nimrod igneous province, the presence of which is corroborated by aeromagnetic data (Goodge and Finn, 2010) and consistent with the new age and isotopic data presented here. Figure 16 shows the inferred distribution of the Nimrod Complex (based on extrapolation of aeromagnetic anomalies covering exposures of this metamorphic terrain), the locations of sampled glacial moraines formed during ice flow through the mountain range, and the adjacent subglacial Nimrod igneous province as inferred from high-amplitude, positive aeromagnetic anomalies and across which ice flow occurs. Goodge and Finn (2010) speculated that the most likely sources for the observed high-amplitude, positive magnetic anomalies were Fe-rich A- or I-type granites

or orthogneisses, perhaps associated with underplated mafic lower crustal rocks, exemplified by Mesoproterozoic granitoid intrusions of southwestern Laurentia. Coupled with their Hf-isotope compositions and inferred source ages, the glacial clast age data thus provide a new portrait of East Antarctic crust in which a significant tract of composite Proterozoic igneous crust, not exposed anywhere else, was formed during punctuated magmatic events representing regional crustal domains of ~1.5, 1.85, and 2.7 Ga age.

The dominance of Proterozoic crust in central East Antarctica is further illustrated in Figure 17, which compares the ages of the dated glacial clasts with known events in exposed basement of the nearby Nimrod Complex, distinctive ages of Proterozoic crust formation in Laurentia, and the provenance signatures of detrital zircon ages from sedimentary and metasedimentary rocks exposed in the central Transantarctic Mountains. As noted earlier, the clast ages do not overlap with known crystalline basement in the region (Fig. 17a). There are, however, age similarities to both the Grenville and A-type granite provinces in Laurentia (or North American, NA). Particularly noteworthy are the age distributions of detrital zircons in sedimentary assemblages that have sources in cratonic East Antarctica. First, the significant Proterozoic makeup of crust in the interior of central East Antarctica is well-illustrated by the detrital zircon age record from Neoproterozoic rift-margin strata from this region (Fig. 17b). A composite detrital age signature obtained from the Beardmore Group with a cratonic provenance shows that the interior region of East Antarctica is underlain mainly by 900-2200 Ma crust (Goodge et al., 2002, 2004; Myrow et al., 2002; Goodge and Fanning, 2016). There is a remarkable correspondence between the discrete ages found among the sampled granitoid clast types and the age probability distribution shown by a large composite population of detrital zircon ages from the Beardmore Group, with significant peaks of about 1170, 1540, 1800 and 2510 Ma. Together, the limited but sample-specific glacial igneous clast results mimic the age pattern captured by the averaging process associated with detrital mineral deposition along the cratonic rift margin. In contrast, both the glacial clast ages and detrital zircon ages from Neoproterozoic strata differ from the detrital zircon age distribution obtained from high-grade

metasedimentary rocks associated with the Nimrod Complex basement terrain exposed near the glacial sample sites (Fig. 17c; Goodge and Fanning, 2016). The latter age distribution from the Argosy Schists indicates primarily local sources within gneisses and orthogneisses of the Nimrod Complex (shown by vertical purple bars in Fig. 17), with discrete age groupings of about 1720, 2500 and 3100 Ma, and only minor contributions from <1700 Ma Proterozoic sources. Thus, the exposed basement terrain represented by the Nimrod Complex and associated Argosy Schist units thus is dominated by Paleoproterozoic to Mesoarchean igneous and metamorphic rocks, whereas the deeper, ice-covered interior of the East Antarctic shield is likely comprised mostly by Paleo- to Mesoproterozoic crust <2000 Ma.

Figure 18 shows the broader context with regard to source area of the glacial clasts. The Byrd Glacier drainage covers a large region of central East Antarctica, with ice divides extending to Dome A and Dome C. Fast flow in the Byrd outlet of >800 m a^{-1} (Stearns et al., 2008) allows ice in this catchment to drain rapidly through the Transantarctic Mountains, accompanied by slower flow in other ice streams feeding the Nimrod and Beardmore glaciers. Based on the ice velocity field from Rignot et al. (2011) and the locations of our sample sites relative to the Byrd outlet, the combined potential source area for the clasts in this study is shown in Figure 18. Most of the ice flows through the Byrd Glacier outlet itself, stranding moraine material at Lonewolf Nunataks, whereas other sites are sourced from smaller sub-streams. The total possible source area represented by these clasts therefore reaches high into the Byrd catchment and possibly onto the southwestern flank of the Gamburtsev Subglacial Mountains (GSM). The GSM are a tectonically enigmatic subglacial mountain massif that preserves an intricate and ancient fluvial landscape (Rose et al., 2013). This interior mountain massif is unique because of its geographic isolation, thick crustal root, apparent lack of Phanerozoic activity, and its importance as the interior highland on which the East Antarctic ice sheet began to form at ~34 Ma (DeConto and Pollard, 2003; Bo et al., 2009). Seismic tomography and velocity inversion results indicate that the GSM are underlain by crust >55-60 km thick and have a lithospheric root about 250 km thick (Heeszel et al., 2013; An et al., 2015), consistent with an orogenic origin. Comparison of the phase velocity structure beneath the GSM

with orogenic provinces worldwide, however, shows that the GSM are most similar to Archean and Paleoproterozoic cratons (Heeszel et al., 2013). Ferraccioli et al. (2011) suggested that the GSM formed as part of a late Mesoproterozoic (~1 Ga) orogeny that was rejuvenated during Permian and Cretaceous rifting. The age and isotopic data from this study therefore indicate that a potentially wide swath of Proterozoic crust underlies the central East Antarctic ice sheet, and that a Proterozoic origin for the GSM is likely. In particular, abundant evidence of Grenvillian (1200-1130 Ma) metamorphic overprinting and deformation of clasts with magmatic ages >1200 Ma, and preservation of Grenvillian igneous ages of 1100-1060 Ma (Goodge et al., 2010), are consistent with models invoking a Mesoproterozoic origin for the GSM.

Age and isotopic comparison with Australia and Laurentia

The multiple Proterozoic age groups from ice-covered East Antarctica can be compared isotopically with provinces of similar age in Australia and southwestern Laurentia in order to test paleogeographic correlations prior to ~1 Ga. Figure 19 shows the initial ε_{Hf} compositions of the Antarctic glacial clasts as a function of age, compared to rock units in southern Australia and southwestern Laurentia with similar age and crustal setting. In particular, comparison with the Gawler Craton in southern Australia is warranted because of its close age and petrotectonic affinity with geologic units in the Terre Adélie Craton and the Nimrod Complex (see Goodge and Fanning, 2016). Likewise, similarities in ages of the Nimrod Complex, detrital zircons from rift-margin successions, and glacial clasts relative to basement units in the Mojave, Yavapai-Mazatzal, and granite-rhyolite provinces of southwestern Laurentia (Goodge et al., 2001, 2004, 2008, 2010; Goodge and Fanning, 1999, 2016) indicate an age association among crustal units that can be tested by comparison of zircon isotopic composition.

Glacial clasts with ages of ca. 2010, 1860, 1790, and 1570 Ma (Goodge et al., 2010, this study), as well as basement igneous and metamorphic ages of ~1.7 Ga from the Nimrod Complex, have initial ε_{Hf} compositions that are quite similar to age-equivalent units of the Gawler Craton (e.g., Miltalie gneiss, Donington Suite, Kimban Orogen, and Hiltaba Suite; Fanning et al., 2007; Hand et al., 2007; Reid et al.,

2008; Belousova et al., 2009; Howard et al., 2011). Notably, the ca. 2010 and 1570 Ma clasts from this study have similar ages and isotopic compositions as the ca. 2010 Ma Miltalie gneiss and ca. 1590 Ma Hiltaba granites, suggesting a common origin. The Hiltaba intrusions and co-magmatic Gawler Range Volcanics (1595-1575 Ma), that together are a hallmark of the Gawler craton, have a direct counterpart in ~1.6 Ga rhyodacite and rhyolite clasts found in glacial moraines in Terre Adélie (Peucat et al., 2002). The Terre Adélie clasts are high-K alkali-calcic volcanic rocks with similar age, petrographic and geochemical characteristics as the Gawler Range Volcanics, including whole-rock ε_{Nd} of 0 to +1 and T_{DM} of about 2 Ga. Geochemically, our sample from Group 3 is very similar in major and trace element composition to the felsic volcanics from Terre Adélie (Fig. 4), and its initial ε_{Hf} is similar to rocks from the Hiltaba Suite and Gawler Range Volcanics (Fig. 19). These data indicate that the distinctive ~1.6 Ga magmatic elements of the Gawler Craton indeed extend beyond the Terre Adélie coast into central East Antarctica. Together with evidence of ~1.7 Ga magmatism and orogenic activity in the Nimrod Complex, the correlated glacial clasts affirm the southward regional extent of the Mawson Continent (Goodge and Fanning, 2016).

The Proterozoic record provided by the igneous glacial clasts also resembles distinctive episodes of magmatic crust formation in Laurentia. For example, the ca. 1860 Ma clasts are strikingly similar in their Hf-isotope composition to igneous components of similar age in the Clearwater metamorphic complex in northern Idaho. Orthogneisses in the Clearwater complex show a bimodal age distribution, with Neoarchean rocks ranging in age from 2.67-2.65 Ga and Paleoproterozoic intrusions with ages of 1.88-1.84 Ga (Fisher et al., 2013, 2014; Wang et al., 2014; Vervoort et al., 2016b). The ~1.86 Ga Idaho orthogneisses have a wide range of initial ε_{Hf}, from about -8 to +8 (Fig. 19), consistent with mixing between a juvenile depleted mantle end-member and the pre-existing 2.65 Ga crust that their protoliths intruded. The ca. 1860 Ma samples in this study (Group 5) show a similar distribution of initial ε_{Hf} that indicates mixing with pre-existing Neoarchean crust of about 2.7 Ga age. The similarity in ages and isotopic composition between Group 5 clasts and rocks of the Clearwater complex thus provide a

potentially unique way to correlate igneous events in Laurentia and East Antarctica related to consolidation of the Columbia supercontinent. Age correspondence with ca. 1850 Ma granitoids of the Donington Suite in Australia (initial ε_{Hf} ranging from 0 to +2; Reid et al., 2008) may expand this connection to include the Gawler Craton. Likewise, our ~1570 Ma sample from Group 3 is isotopically similar to a 1578 Ma augen gneiss from the Priest River complex of northern Idaho with initial ε_{Hf} = -6.2 (Evans and Fischer, 1986; C.M. Fisher, unpubl. data); the Priest River unit is from the same area as the 1577 Ma Laclede gneiss (Doughty et al., 1998) that falls within the so-called North American magmatic gap and serves as a distinctive time marker.

The glacial clasts from East Antarctica also have counterparts in the ~1.4 Ga Laurentian granite province (Goodge and Vervoort, 2006; Wooden et al., 2013) and ~1.2 Ga igneous and gneissic rocks from the Mojave province and basement uplifts in New Mexico (Ramo et al., 2003; Wooden et al., 2013). As shown by Goodge and Vervoort (2006), the distinctive Laurentian granites show Hf-isotopic compositions related to the age and ancestry of crust with which they interacted, however all samples studied show radiogenic compositions with initial $\varepsilon_{Hf} > 0$. The glacial clasts of this age, including our new samples in this study from Group 2 and sample TNQ of Goodge et al. (2008), are notably more radiogenic ($\varepsilon_{Hf} > +6$) but overlap with the Laurentian population, especially those of the southern Granite-Rhyolite province. As noted earlier, the mineralogical, textural, geochemical, and isotopic similarities of this large population of ~1.4 Ga glacial clasts with the distinctive Laurentian magmatic belt provide compelling evidence that the crust of central East Antarctica includes a sizeable component of granites that correlate in age and origin with counterparts in southwestern Laurentia. Such a correlation, made earlier by Goodge et al. (2008), explains how the prominent Laurentian belt terminates abruptly along the Neoproterozoic rift margin of southwestern Laurentia and continued into a once contiguous East Antarctica.

Last, a suite of rocks with ages of ~1.2 Ga occur in both the Mojave Desert area of eastern California and extend to southwestern New Mexico as part of the so-called anorthosite-mangerite-charnockite-granite (AMCG) belt that cuts across southwestern Laurentia. One suite of charnockite, syenite, and

granite in the San Gabriel and Eagle mountains of eastern California has average initial ε_{Hf} compositions of +3 to +5 (Wooden et al., 2013), explained as mixing of crust and mantle melt components. A second suite of tholeiitic A-type granite-anorthosite intrusions in the Mazatzal province of southwestern New Mexico has average initial ε_{Nd} compositions of about +2 (Ramo et al., 2003), which corresponds to initial ε_{Hf} = +5 (Vervoort et al., 2011). These intrusions are interpreted as the result of magmatic underplating beneath pre-existing juvenile Paleoproterozoic lower crust. The two samples from Group 1 with ages of ca. 1210 Ma have nearly identical initial ε_{Hf} compositions of +3 to +4 (Fig. 19). The co-occurrence of ca. 1.4 and 1.2 Ga igneous rocks in both Mojave- and Mazatzal-type crust, and the presence of glacially-sourced rocks with similar age and isotopic compositions, strengthens ties between East Antarctica and southwestern Laurentia to at least this time period.

In addition to the broad span of Proterozoic igneous events recorded by this glacial clast suite between ca. 2.0-1.2 Ga, a number of samples show evidence of metamorphism and/or deformation between 1200-1130 Ma. An earlier study of glacially-sourced Proterozoic igneous clasts also documented preservation of Grenvillian igneous ages of 1100-1060 Ma (Goodge et al., 2010). Orogenic and magmatic activity thus inferred for central East Antarctica during these time periods is coeval with events in the Grenville Orogen of Laurentia, with the ages of metamorphism in basement of Western Tasmania (Berry et al., 2008), and with recently recognized metamorphic and igneous activity in western North America (see Milidragovic et al., 2011). Despite older Proterozoic ties between East Antarctica and the Gawler Craton, Grenville-age activity is not recognized in the Gawler, indicating a marked difference in its Mesoproterozoic history that may reflect a more stable, interior cratonic position. Lacking isotopic tracer data for the other occurrences in Tasmania and Laurentia, it is not possible to unambiguously test specific age correlations between these areas. However, the finding of Grenvillian activity in central East Antarctica provides further evidence of tectonism related to the final assembly of Rodinia among the cratonic elements discussed here.

The new ages and isotopic compositions from igneous rocks of the East Antarctic interior, as indicated by the glacial clasts described here, have clear counterparts in key Proterozoic crustal provinces of southern Australia and southwestern Laurentia (Fig. 20). Together, these age and isotopic correlations lend credence to the concept of a paleogeographically-linked cratonic assemblage that records development of the Columbia supercontinent between ca. 2000-1800 Ma, intra-cratonic or craton-margin tectonism between 1850-1450 Ma, and Mesoproterozoic intra-cratonic magmatism at ca. 1450 and 1220 Ma culminating in the assembly of Rodinia. This long-lived association of central East Antarctica, southern Australia, and southwestern Laurentia during the evolution of Columbia and Rodinia is further supported by the correlation of distinctive ~1.6 Ga volcanic breccias and associated IOCG deposits in the Wernecke Mountains of Yukon in northwestern Canada and in the Olympic Dam area of eastern Australia (e.g., Thorkelson et al., 2001a,b; Furlanetto et al., 2016). The age and isotopic signatures shared between central East Antarctica, southwestern Laurentia, and southern Australia thus attest to the assembly and relative continuity of a Proterozoic supercontinent that persisted between about 2.0 and 1.2 Ga prior to rifting and eventual breakup in the late Neoproterozoic (see also, Goodge et al., 2004, 2008; Medig et al., 2014; Mulder et al., 2015; Goodge and Fanning, 2016).

The general reconstruction shown in Figure 20 emphasizes that core parts of East Antarctica within the Mawson Continent were aligned with crustal provinces in present-day southwestern Laurentia, and that cratonic rocks in southern and central Australia correlate with geology exposed in the northern Cordillera, particularly in Yukon. A host of data support this configuration, including correlation of igneous and metamorphic basement geology, distinctive igneous isotopic signatures, sedimentary provenance relations, detrital zircon isotopic signatures, distinctive IOCG mineralization, and paleomagnetism (see, for example, Goodge et al., 2001, 2004, 2008, 2010; Thorkelson et al., 2001a,b; Fanning, 2003; Zhao et al., 2004; Link et al., 2007; Payne et al., 2009; Stewart et al., 2010; Daniel et al., 2013; Furlanetto et al., 2013, 2016; Halpin et al., 2014; Medig et al., 2014; Pisarevsky et al., 2014; Mulder et al., 2015; Thorkelson and Laughton, 2016). Some earlier models suggested that parts of central

Australia aligned with southwestern Laurentia (e.g., Brookfield, 1993; Burrett and Berry, 2000; Karlstrom et al., 2001; Berry et al., 2008; Gibson et al., 2008, 2012). Based on unique piercing points represented by petrologic, age, and isotopic data, however, these models are demonstrably not tenable. Such paleogeographic relationships do not take into account what is likely to be the single-most unique correlation between East Antarctica and Laurentia – that of the nearly-continuous belt of petrographically, geochemically, and isotopically distinctive ca. 1.45 Ga intrusions crossing Laurentia which terminates abruptly at its late Neoproterozoic rift margin. Numerous identical clasts are found in glacial tills sourced in East Antarctica but do not occur, for example, in Australia. Furthermore, the AUSWUS-type reconstructions do not account for similarities between ca. 1.59 Ga igneous and mineralization events that link the Gawler-Curnamona craton and Olympic Dam-type deposits with the mineralized Wernecke breccia and associated rocks in Yukon. Therefore, a general model like that shown in Fig. 20 best fits the direct correlations between central East Antarctica and southwestern Laurentia, and simultaneously is supported by correlations between southern-central Australia and the northern Laurentian Cordillera.

Implications for Proterozoic paleogeography in Columbia-Nuna and Rodinia

The new age and isotopic results presented here for igneous rocks from central East Antarctica add perspective to our understanding of Proterozoic paleogeography during development of the Columbia-Nuna and Rodinia supercontinents. As shown in Figure 21, which compares key Proterozoic orogenic, depositional and magmatic events in East Antarctica, Australia and Laurentia, the three cratonic regions share a common history between about 1.85 and 1.06 Ga. A punctuated sequence of geotectonic events linking these regions is shown not only by strikingly similar ages of orogenic, depositional, and igneous events, but by correlated radiogenic isotope tracer compositions in igneous units of unique age and character, as well as sedimentary provenance connections between source and basin. Key associations include: (1) Hf-isotope correlation of distinctive igneous rocks in central East Antarctica, Gawler Craton, and northern Idaho region of Laurentia (Clearwater Complex and Laclede gneiss) between 2.01 and 1.57 Ga; (2) geochemical and isotopic correlation of ca. 1.45 Ga ferroan or A-type granitoids in central East

Antarctica and southwestern Laurentia; (3) episodic Grenvillian events in all three cratonic regions, including isotopically similar granitoids from central East Antarctica and the Mojave/New Mexico region of southwestern Laurentia; and (4) sedimentary provenance linkages from both detrital-zircon age populations and radiogenic isotope tracers that connect ca. 1.59 and 1.45 Ga sources in East Antarctica and Gawler Craton with deposition in Antarctic marginal basins (Beardmore Group), Tasmania (Rocky Cape Group), and several basins in western Laurentia (Wernecke, Belt-Purcell, Lemhi, Hess Canyon, Trampas, Ortega, etc.). Taken altogether, these persistent and uniquely identifiable correlations — so-called piecing points — attest to a long-lived cratonic association that starts with nucleation of the Columbia-Nuna supercontinent between about 2.01-1.85 Ga and continues through a temporally correlated and spatially related series of events leading to eventual assembly of Rodinia by about 1.1 Ga.

The paleogeographic associations described above are not meant to convey that the cratonic elements represented by modern-day central East Antarctica, central-southern Australia, and western Laurentia were geometrically fixed to one another during this period between 2.0-1.0 Ga. Other studies indicate that discrete periods in this Proterozoic history were marked by extension, basin development, growth of volcanic arcs, and convergent-margin orogenesis (see Betts et al., 2008). For example, arc-type plutonic and volcanic rocks of the ca. 1.7 Ga Bonnetia arc (Bonnet Plume River intrusions and Slab volcanics; Thorkelson et al., 2001a; Furlanetto et al., 2013) mark a period of oceanic convergence between northwestern Laurentia and northern Australia prior to collapse and arc accretion by about 1650-1600 Ma. Likewise, the ca. 1.7 Ga Nimrod-Kimban orogenic events appear related to crustal thickening associated with amalgamation of existing cratonic blocks to form the Mawson Continent (Goodge et al., 2001; Betts and Giles, 2006; Payne et al., 2009; Goodge and Fanning, 2016). Differential movement between major cratonic blocks appears to have involved opening of marine basins and later closure during formation and obduction of magmatic-arc crust (e.g., Furlanetto et al., 2013). This Paleoproterozoic tectonic activity may have been accommodated by segments of attenuated crust, arcs, and micro-ribbons of continental crust (Betts et al., 2008), as part of a diffuse orogenic system. Nonetheless, the periodic but persistent

linkages between these cratonic regions indicates that they maintained relatively close proximity, at least sufficient to allow for inter-cratonic geological connection over time.

SUMMARY

The study of sedimentary and glacial detritus can help to inform the ages, compositions, and cooling histories of crust from the interior of East Antarctica (e.g., Peucat et al., 2002; Goodge et al., 2008, 2010; van de Flierdt et al., 2008; Goodge and Fanning, 2010; Pierce et al., 2011). In this study, new SHRIMP U-Pb zircon ages from a large suite of granitoid clasts collected from glacial catchments draining central East Antarctica through the Transantarctic Mountains show that at least parts of the crust in this ice-covered region was formed by a series of magmatic events at ~2.0, 1.9, ~1.8, ~1.6, 1.5-1.4, and 1.2-1.1 Ga. The dominant granitoid populations are ca. 1880-1850, 1500-1450 and 1210-1060 Ma. None of these igneous ages are known from rock exposures in the region. Zircon Hf and O isotopic compositions from this suite have variable compositions that indicate both juvenile, mantle-derived melts and those involving mixtures of older crustal sources. The older granitoids (2.0-1.8 Ga) were derived primarily as mixtures of juvenile components and contributions from older, pre-existing crust formed between about 2.7-2.1 Ga; melts formed at about 1.5 Ga have juvenile, mantle-like isotopic compositions, whereas those formed at about 1.2 Ga were derived primarily from pre-existing crust, possibly by re-melting of 1.5 Ga sources.

The age and isotopic data from these glacially-eroded granitoids provide a first glimpse of the crustal growth history in central East Antarctica and suggest a punctuated history of Proterozoic magmatic and crustal growth events chiefly at ~2.7, ~1.8, and ~1.5 Ga. Furthermore, the glacial clast ages are similar to detrital-zircon provenance in Neoproterozoic rift-margin strata that have major age populations of 1.88-1.72, 1.64-1.36, and 1.28-1.04 Ga, strengthening a case for episodic Proterozoic magmatic growth of East Antarctic crust. Together, the local basement and clast ages indicate the presence in central East Antarctica of a large, composite Archean-Proterozoic craton that reflects crustal growth within the core of

East Gondwana. Correlation with the Gawler craton of Australia is confirmed by zircon isotopic compositions at 2.02, 1.85, 1.57, and 1.21 Ga. Age and isotopic data from 1.85, 1.46 and 1.21 Ga glacial materials derived from East Antarctic crust correlate with provinces in Laurentia (Idaho-Medicine Hat, Yavapai-Mazatzal-granite, and Grenville-Mojave, respectively), thereby providing direct geologic support for a SWEAT-type configuration linking these cratonic provinces during evolution of the Columbia and Rodinia supercontinents. Abundant ~1.2-1.1 Ga igneous and metamorphic clasts may sample crust underlying the Gamburtsev Subglacial Mountains and indicate the presence of Grenvillian orogenic belts in the interior that played a role in Rodinia assembly.

Acknowledgements. Field and analytical portions of this project were supported by the National Science Foundation (award 0944645). We are grateful for the help of many individuals on this project. Dylan Taylor and Tanya Dreyer were valuable parts of the field team. Michael Buschette, Tanya Dreyer, Angela Hawkins, Robert Kryzer and Amy Radakovich assisted with sample preparation (sample processing, imaging, analysis). Bryan Bandli supported imaging and analysis in the Research Instrumentation Lab at UMD. Shane Paxton prepared the mineral separations and Bin Fu made sample mounts at ANU. Victor Valencia and Charles Knack helped with the isotope analyses at WSU. Jacqueline Halpin and Derek Thorkelson provided thorough reviews of the manuscript and inspired valuable new perspectives.

References

Aitken, A.R.A., Young, D.A., Ferraccioli, F., Betts, P.G., Greenbaum, J.S., Richter, T.G., Roberts, J.L., Blankenship, D.D., Siegert, M.J., 2014. The subglacial geology of Wilkes Land, East Antarctica. *Geophysical Research Letters,* 41, doi:10.1002/2014GL059405.

Amelin, Y., Lee, D.-C., Halliday, A.N., 2000. Early-middle Archaean crustal evolution deduced from Lu-Hf and U-Pb isotopic studies of single zircon grains. *Geochimica et Cosmochimica Acta*, 64(24), 4205–4225.

An, M., Wiens, D.A., Zhao, Y., Feng, M., Nyblade, A.A., Kanao, M., Li, Y., Maggi, A., Lévêque, J.-J., 2015. S-velocity model and inferred Moho topography beneath the Antarctic Plate from Rayleigh waves. *Journal of Geophysical Research Solid Earth,* 120, 359–383, doi:10.1002/ 2014JB011332.

Anderson, J.L., 1983. Proterozoic anorogenic granite plutonism of North America. In: Medaris, L.G.J., Byers, C.W., Mickelson, D.M., Shanks, W.C. (Eds.), *Proterozoic Geology; Selected Papers from an International Proterozoic Symposium*, Memoir of the Geological Society of America, 161, Geological Society of America, Boulder, Colorado, pp. 133–152.

Anderson, J.L., Bender, E.E., 1989. Nature and origin of Proterozoic A-type granitic magmatism in the southwestern United States. *Lithos,* 23, 19–52.

Anderson, J.L., Cullers, R.L., 1999. Paleo- and Mesoproterozoic granite plutonism of Colorado and Wyoming. *Rocky Mountain Geology,* 34, 149–164.

Anderson, J.L., Morrison, J., 2005. Ilmenite, magnetite, and peraluminous Mesoproterozoic anorogenic granites of Laurentia and Baltica. *Lithos*, 80, 45–60.

Belousova, E.A., Reid, A.J., Griffin, W.L., O'Reilly, S.Y., 2009. Rejuvenation vs. recycling of Archean crust in the Gawler Craton, South Australia: Evidence from U–Pb and Hf isotopes in detrital zircon. *Lithos*, 113, 570-582.

Berry, R.F., Steelab, D.A., Meffrea, S., 2008. Proterozoic metamorphism in Tasmania: Implications for tectonic reconstructions. *Precambrian Research*, 166, 387-396.

Betts, P.G., Giles, D., Lister, G.S., Frick, L.R., 2002. Evolution of the Australian lithosphere. *Australian Journal of Earth Sciences*, 49, 661–695.

Betts, P.G., Giles, D., 2006. The 1800–1100 Ma tectonic evolution of Australia. *Precambrian Research*, 144, 92–125.

Bo, S., Siegert, M.J., Mudd, S.M., Sugden, D., Fujita, S., Xiangbin, C., Yunyun, J., Xueyuan, T., Yuansheng, L., 2009. The Gamburtsev Mountains and the origin and early evolution of the Antarctic Ice Sheet. *Nature*, 459, 690–693.

Boger, S.D., 2011. Antarctica — Before and after Gondwana. *Gondwana Research* 19 (2), 335-371.

Bouvier, A., Vervoort, J.D., Patchett, P.J., 2008. The Lu–Hf and Sm–Nd isotopic composition of CHUR: Constraints from unequilibrated chondrites and implications for the bulk composition of terrestrial planets. *Earth and Planetary Science Letters*, 273, 48-57, doi.org/10.1016/j.epsl.2008.06.010.

Brookfield, M.E., 1993. Neoproterozoic Laurentia–Australia fit. *Geology*, 21, 683–686.

Burrett, C., Berry, R., 2000. Proterozoic Australia–western United States (AUSWUS) fit between Laurentia and Australia. *Geology*, 28, 103–106.

Chauvel, C., Garçon, M., Bureau, S., Besnault, A., Jahn, B., Ding, Z., 2014. Constraints from loess on the Hf–Nd isotopic composition of the upper continental crust. *Earth and Planetary Science Letters*, 388, 48-58.

Condie, K.C., Aster, R.C., 2010. Episodic zircon age spectra of orogenic granitoids: The supercontinent connection and continental growth. *Precambrian Research*, 180, 227–236, doi:10.1016/j.precamres.2010.03.008.

Condie, K.C., Belousova, E., Griffin, W.L., Sircombe, K.N., 2009. Granitoid events in space and time: Constraints from igneous and detrital zircon age spectra. *Gondwana Research*, 15, 228- 242.

Daly, S.J., Fanning, C.M., Fairclough, M. C., 1998. Tectonic evolution and exploration potential of the Gawler Craton, South Australia. *J. Aust. Geol. Geophys.*, 17, 145–168.

Daniel, C.G., Pfeifer, L.S., Jones, J.V., 2013. Detrital zircon evidence for non-Laurentian provenance, Mesoproterozoic (ca. 1490–1450 Ma) deposition and orogenesis in a reconstructed orogenic belt, northern New Mexico, USA: defining the Picuris orogeny. *Geological Society of America Bulletin*, 125, 1423–1441.

Davidson, J.P., McMillan, N.J.M., Moorbath, S., Wörner, G., Harmon, R.S., López-Escobar, L., 1990. The Nevados de Payachata volcanic region (18°S/69°W, N. Chile) II. Evidence for widespread crustal involvement in Andean magmatism. *Contributions to Mineralogy and Petrology*, 105, 412–432.

Davidson, J.P., Harmon, R.S., Wörner, G., 1991. The source of central Andean magmas: Some considerations. *In* Harmon, R.S., and Rapela, C.W. (Eds.), *Andean Magmatism and Its Tectonic Setting*, Geological Society of America Special Paper, 265, 233–244.

DeConto, R.M., Pollard, D., 2003. Rapid Cenozoic glaciation of Antarctica induced by declining atmospheric CO_2. *Nature*, 421, 245-249.

Doughty, P.T., Chamberlain, K.R., 2008. Protolith age and timing of Precambrian magmatic and metamorphic events in the Priest River complex, northern Rockies. *Canadian Journal of Earth Sciences*, 45(1), 99-116, doi.org/10.1139/e07-067.

Doughty, P.T., Price, R.A., Parrish, R.R., 1998. Geology and U-Pb geochronology of Archean basement and Proterozoic cover in the Priest River Complex, northwestern United States, and their implications for Cordilleran structure and Precambrian continent reconstructions. *Canadian Journal of Earth Sciences*, 35, 39–54.

Evans, K.V., Fischer, L.B., 1986. U–Th–Pb geochronology of two augen gneiss terranes, Idaho: new data and tectonic implications. *Canadian Journal of Earth Sciences*, 23, 1919–1927.

Fanning, C.M., 2003. Detrital zircon provenance of the Mesoproterozoic Pandurra Formation, South Australia: Gawler Craton zircon population and implications for the Belt Supergroup. Geological Society of America *Abstracts with Programs*, 35(6), 465.

Fanning, C.M., Reid, A.J., Teale, G.S., 2007. A geochronological framework for the Gawler Craton, South Australia. South Australia Geological Survey, Bulletin 55, 258 pp.

Ferraccioli, F., Finn, C.A., Jordan, T.A., Bell, R.E., Anderson, L.M., Damaske, D., 2011. East Antarctic rifting triggers uplift of the Gamburtsev Mountains. *Nature*, 479, 388-391, doi.10.1038/nature10566.

Finn, C.A., Sims, P.K., 2005. Signs from the Precambrian: The geologic framework of Rocky Mountain region derived from aeromagnetic data, in Karlstrom, K.E., and Keller, G.R. (Eds.), *The Rocky Mountain Region; An Evolving Lithosphere: Tectonics, Geochemistry, and Geophysics*, American Geophysical Union, Geophysical Monograph Series, Washington, D. C., 154, 39–54.

Fisher, C.M., Vervoort, J.D., Jansen, A.C., Lewis, R.S, Gaschnig, R.M., Goodge, J.W., 2013. Precambrian crystalline basement rocks of northwest Laurentia: Constraining the formation and evolution of North America. *Geological Society of America Abstracts with Programs*, 45(7), 310.

Fisher, C.M., Vervoort, J.D, Lewis, R.S., Gaschnig, R.M., Goodge, J., Jansen, A.C, Wang, D., 2014c. A

bimodal belt of ~1.86 to 2.66 Ga tonalitic gneisses in northwest Laurentia: U-Pb and Lu-Hf constraints on the evolution of North America. *Geological Society of America Abstracts with Programs*, 46(5), 19.

Fitzsimons, I.C.W., 2003. Proterozoic basement provinces of southern and southwestern Australia, and their correlation with Antarctica. In: Yoshida, M., Windley, B.F., and Dasgupta, S. (Eds.), *Proterozoic East Gondwana; supercontinent assembly and breakup*: London, Geological Society of London Special Publication, 206, pp. 93-130.

Fretwell, P., et al., 2013. Bedmap2: Improved ice bed, surface and thickness datasets for Antarctica. *Cryosphere*, 7, 375–393, doi:10.5194/tc-7-375-2013.

Frost, B.R., Barnes, C.G., Collins, W.J., Arculus, R.J., Ellis D.J., Frost, C.D., 2001. A geochemical classification for granitic rocks. *Journal of Petrology*, 42(11), 2033-2048, doi: 10.1093/petrology/42.11.2033.

Frost, C.D., Frost, B.R., 2011. On ferroan (A-type) granitoids: their compositional variability and modes of origin. *Journal of Petrology*, 52, 39-53, doi:10.1093/petrology/egq070.

Furlanetto, F., Thorkelson, D.J., Gibson, H.D., Marshall, D.D., Rainbird, R.H., Davis, W.J., Crowley, J.L., Vervoort, J.D., 2013. Late Paleoproterozoic terrane accretion in northwestern Canada and the case for circum-Columbian orogenesis. *Precambrian Research,* 224, 512–528.

Furlanetto, F., Thorkelson, D.J., Rainbird, R.H., Davis, W.J., Gibson, H.D., Marshall, D.D., 2016. The Paleoproterozoic Wernecke Supergroup of Yukon, Canada: Relationships to orogeny in northwestern Laurentia and basins in North America, East Australia, and China. *Gondwana Research*, 39, 14–40.

Gerdes, A., Zeh, A., 2009. Zircon formation versus zircon alteration — New insights from combined U–Pb and Lu–Hf in-situ LA-ICP-MS analyses, and consequences for the interpretation of Archean zircon from the Central Zone of the Limpopo Belt. *Chemical Geology*, 261, 230–243

Gernon, T.M., Hincks, T.K., Tyrrell, T., Rohling, E.J., Palmer, M.R., 2016. Snowball Earth ocean chemistry driven by extensive ridge volcanism during Rodinia breakup. *Nature Geoscience*, 9, 242-248, doi:10.1038/NGEO2632.

Gibson, G.M., Rubenach, M.J., Neumann, N.L., Southgate, P.N., Hutton, L.J., 2008. Syn- and post-extensional tectonic activity in the Palaeoproterozoic sequences of Broken Hill and Mount Isa and its bearing on reconstructions of Rodinia. *Precambrian Research*, 166, 350–369.

Gibson, G.M., Henson, P.A., Neumann, N.L., Southgate, P.N., Hutton, L.J., 2012. Paleoproterozoic–earliest Mesoproterozoic basin evolution in the Mount Isa region, northern Australia and implications for reconstructions of the Nuna and Rodinia supercontinents. *Episodes*, 35, 131–141.

Goodge, J.W., Fanning, C.M., 1999. 2.5 billion years of punctuated Earth history as recorded in a single rock. *Geology*, 27, 1007-1010.

Goodge, J.W., Fanning, C.M., 2016. Mesoarchean and Paleoproterozoic history of the Nimrod Complex, central Transantarctic Mountains, Antarctica: Stratigraphic revisions and relation to the Mawson Continent in East Gondwana. *Precambrian Research*, 285, 242-271, doi:10.1016/j.precamres.2016.09.001.

Goodge, J.W., Fanning, C.M., Bennett, V.C., 2001. U-Pb evidence of ~1.7 Ga crustal tectonism during the Nimrod Orogeny in the Transantarctic Mountains, Antarctica: implications for Proterozoic plate reconstructions. *Precambrian Research*, 112, 261-288.

Goodge, J.W., Fanning, C.M., Brecke, D.M., Licht, K.J., Palmer, E.F., 2010. Continuation of the Laurentian Grenville province in western East Antarctica. *Journal of Geology*, 118, 601-619, doi:10.1086/656385.

Goodge, J.W., Fanning, C.M., Norman, M., Bennett, V.C., 2012. Temporal, isotopic and spatial relations of early Paleozoic Gondwana-margin arc magmatism, central Transantarctic Mountains, Antarctica. *Journal of Petrology*, doi:10.1093/petrology/egs043.

Goodge, J.W., Finn, C.A., 2010, Glimpses of East Antarctica: Aeromagnetic and satellite magnetic view from the central Transantarctic Mountains of East Antarctica. *Journal of Geophysical Research Solid Earth,* 115, 1-22, B09103, doi: 10.1029/2009JB006890.

Goodge, J.W., Myrow, P., Williams, I.S., Bowring, S., 2002. Age and provenance of the Beardmore Group, Antarctica: Constraints on Rodinia supercontinent breakup. *Journal of Geology*, 110, 393-406.

Goodge, J.W., Vervoort, J.D., 2006. Origin of Mesoproterozoic A-type granites in Laurentia: Hf isotope evidence. *Earth and Planetary Science Letters*, 243, 711-731; doi:10.1016/j.epsl.2006.01.040.

Goodge, J.W., Vervoort, J.D., Fanning, C.M., Brecke, D.M., Farmer, G.L., Williams, I.S., Myrow, P.M., DePaolo, D.J., 2008. A positive test of East Antarctica-Laurentia juxtaposition within the Rodinia supercontinent. *Science*, 321, 235-240; doi:10.1126/science.1159189.

Goodge, J.W., Williams, I.S., Myrow, P., 2004. Provenance of Neoproterozoic and lower Paleozoic siliciclastic rocks of the central Ross Orogen, Antarctica: Detrital record of rift-, passive- and active-margin sedimentation. *Geological Society of America Bulletin*, 116, 1253-1279.

Halpin, J.A., Daczko, N.R., Clarke, G.L., Murray, K.R., 2013. Basin analysis in polymetamorphic terranes: An example from east Antarctica. *Precambrian Research*, 231, 78–97.

Halpin, J.A., Jensen, T., McGoldrick, P., Meffre, S., Berry, R.F., Everard, J.L., Calver, C.R., Thompson, J., Goemann, K., Whittaker, J.M., 2014. Authigenic monazite and detrital zircon dating from the Proterozoic Rocky Cape Group, Tasmania: Links to the Belt-Purcell Supergroup, North America. *Precambrian Research*, 250, 50–67.

Hand, M., Reid, A., Jagodzinski, L., 2007. Tectonic framework and evolution of the Gawler Craton, Southern Australia. *Economic Geology*, 102, 1377–1395.

Haran, T., Bohlander, J., Scambos, T., Painter, T., Fahnestock, M., 2005 (updated 2013). *MODIS Mosaic of Antarctica 2003-2004 (MOA2004) Image Map, Version 1*, Boulder, Colorado, National Snow and Ice Data Center, doi:10.7265/N5ZK5DM5.

Harley, S.L., Fitzsimons, I.C.W., Zhao, Y., 2013. Antarctica and supercontinent evolution: historical perspectives, recent advances and unresolved issues. In: Harley, S.L., Fitzsimons, I.C.W. and Zhao, Y. (Eds.), *Antarctica and Supercontinent Evolution*, Geological Society, London, Special Publications, 383, pp. 1–34.

Harley, S.L., Kelly, N.M., 2007. Ancient Antarctica; the Archean of the East Antarctic Shield. In: Van Kranendonk, M.J., Smithies, R.H., and Bennett, V.C. (Eds.), *Earth's oldest rocks: Developments in Precambrian Geology*: Netherlands, Elsevier, pp. 149-186.

Hawkesworth, C.J., Cawood, P.A., Dhuime, B., 2016. Tectonics and crustal evolution. *GSA Today*, 26, 4–11, doi:10.1130/GSATG272A.1.

Hawkesworth, C.J., Kemp, A.I.S., 2006. Using hafnium and oxygen isotopes in zircons to unravel the record of crustal evolution. *Chemical Geology*, 226, 144-162.

Heeszel, D.S., Wiens, D.A., Nyblade, A.A., Hansen, S.E., Kanao, M., An, M., Zhao, Y., 2013. Rayleigh wave constraints on the structure and tectonic history of the Gamburtsev Subglacial Mountains, East Antarctica. *Journal of Geophysical Research Solid Earth*, 118, 2138–2153, doi:10.1002/jgrb.50171.

Howard, K.E., Hand, M., Barovich, K.M., Belousova, E., 2011. Provenance of late Paleoproterozoic cover sequences in the central Gawler Craton: Exploring stratigraphic correlations in eastern Proterozoic Australia using detrital zircon ages, Hf and Nd isotopic data. *Australian Journal of Earth Sciences*, 58, 475–500.

Iizuka, I., Hirata, T., Komiya, T., Rino, S., Katayama, I., Motoki, A., Maruyama, S., 2005. U-Pb and Lu-Hf isotope systematics of zircons from the Mississippi River sand: Implications for reworking and growth of continental crust. *Geology*, 33, 485-488, doi: 10.1130/G21427.1.

Jamieson, S.S.R., Sugden, D.E., 2008. Landscape evolution of Antarctica. In: Cooper, A.K., Barrett, P.J., Stagg, H., Storey, B., Stump, E., and Wise, W. (Eds.), *Antarctica: A Keystone in a Changing World* (Proceedings of the 10th International Symposium on Antarctic Earth Sciences): Washington, DC, The National Academies Press, pp. 39-54.

Karlstrom, K.E., Åhäll, K.-I., Harlan, S.S., Williams, M.L., McLelland, J., Geissman, J.W., 2001. Long-lived (1.8–1.0 Ga) convergent orogen in southern Laurentia, its extension to Australia and Baltica, and implications for refining Rodinia. *Precambrian Research,* 111, 5–30.

Kemp, A.I.S., Hawkesworth, C.J., 2014. Growth and differentiation of the continental crust from isotope

studies of accessory minerals. In: Rudnick, R.L. (Ed.), Treatise on Geochemistry 4, *The Crust*, Elsevier Science, Oxford, pp. 379–421.

Kemp, A.I.S., Hawkesworth, C.J., Paterson, B.A., Kinny, P.D., 2006. Episodic growth of the Gondwana supercontinent from hafnium and oxygen isotopes in zircon. *Nature*, 439, 580- 583.

Lindsay, J.F., Brasier, M.D., 2002. Did global tectonics drive early biosphere evolution? Carbon isotope record from 2.6 to 1.9 Ga carbonates of Western Australian basins. *Precambrian Research*, 114, 1–34.

Link, P.K., Fanning, C.M., Lund, K.I., Aleinikoff, J.N., 2007. Detrital zircons, correlation and provenance of Mesoproterozoic Belt Supergroup and correlative strata of east-central Idaho and southwest Montana, *in* Link, P.K., and Lewis, R.S. (Eds.), *Proterozoic geology of western North America and Siberia*. SEPM (Society for Sedimentary Geology) Special Publication 86, 101–128.

Lodders, K., Palme H., Gail, H.P., 2009. Abundances of the elements in the solar system. *In* Trümper, J.E., ed., Landolt-Börnstein - Group VI Astronomy and Astrophysics 4B, Chap. 4.4, Springer Materials, Berlin, Springer-Verlag, 560-630.

Medig, K.P.R., Thorkelson, D.J., Davis, W.J., Rainbird, R.H., Gibson, H.D., Turner, E.C., Marshall, D.D., 2014. Pinning northeastern Australia to northwestern Laurentia in the Mesoproterozoic. *Precambrian Research*, 249, 88-99.

Meert, J.G., 2012. What's in a name? The Columbia (Paleopangaea/Nuna) supercontinent. *Gondwana Research*, 21(4), 987-993.

Milidragovic, D., Thorkelson, D.J., Davis, W.J., Marshall1, D.D., Gibson, H.D., 2011. Evidence for late Mesoproterozoic tectonism in northern Yukon and the identification of a Grenville-age tectonothermal belt in western Laurentia. *Terra Nova*, 23, 307-313, doi: 10.1111/j.1365-3121.2011.01015.x.

Moores, E.M., 2002. Pre-1 Ga (pre-Rodinian) ophiolites: their tectonic and environmental implications. *Geological Society of America Bulletin,* 114, 80–95.

Mulder, J.A., Halpin, J.A., Daczko, N.R., 2015. Mesoproterozoic Tasmania: witness to the East

Antarctica–Laurentia connection within Nuna. *Geology*, 43(9), 759–762, doi:10.1130/G36850.1.

Myrow, P.M., Pope, M.C., Goodge, J.W., Fischer, W., Palmer, A.R., 2002. Depositional history of pre-Devonian strata and timing of Ross Orogenic tectonism in the central Transantarctic Mountains, Antarctica. *Geological Society of America Bulletin,* 114 (9), 1070– 1088.

Nance, R.D., Murphy, J.B., Santosh, M., 2014. The supercontinent cycle: A retrospective essay. *Gondwana* Research, 25, 4-29, doi:10.1016/j.gr.2012.12.026.

Parrish, R.R., Reichenbach, I., 1991. Age of xenocrystic zircon from diatremes of western Canada. *Canadian Journal of Earth Sci*ences, 28, 1232–1238.

Payne, J.L., Hand, M., Barovich, K.M., Reid, A., Evans, D.A.D., 2009. Correlations and reconstruction models for the 2500-1500 Ma evolution of the Mawson Continent. In: Reddy, S.M., Mazumder, R., Evans, D.A.D., Collins, A.S. (Eds.) *Palaeoproterozoic Supercontinents and Global Evolution*, Geological Society, London, Special Publications, 323, pp. 319–355.

Pearce, J.A., Harris N.B.W., Tindle, A.G., 1984. Trace element discrimination diagrams for the tectonic interpretation of granitic rocks. *Journal of Petrology*, 25 (4), 956-983, doi: 10.1093/petrology/25.4.956.

Peucat, J.J., Capdevila, R., Fanning, C.M., Ménot, R.-P., Pécora, L., Testut, L., 2002. 1.60 Ga felsic volcanic blocks in the moraines of the Terre Adélie craton, Antarctica: Comparisons with the Gawler Range volcanics, South Australia. *Australian Journal of Earth Sciences*, 49, 831-845, doi:10.1046/ j.1440-0952.2002.00956.

Pierce, E.L., Williams, T., van de Flierdt, T., Hemming, S.R., Goldstein, S.L., Brachfeld, S.A., 2011. Characterizing the sediment provenance of East Antarctica's weak underbelly: The Aurora and Wilkes sub-glacial basins. *Paleoceanography*, 26, PA4217, doi:10.1029/2011PA002127.

Pisarevsky, S.A., Elming, S.A., Pesonen, L.J., Li, Z.X., 2014. Mesoproterozoic paleogeography: supercontinent and beyond. *Precambrian Research*, 244, 207–225.

Pollard, D., DeConto, R.M., Nyblade, A.A., 2005. Sensitivity of Cenozoic Antarctic ice sheet variations to geothermal heat flux. *Global Planetary Change*, 49, 63–74.

Rämö, O.T., McLemore, V.T., Hamilton, M.A., Kosunen, P.J., Heizler, M., Haapala, I., 2003. Intermittent 1630–1220 Ma magmatism in central Mazatzal province: New geochronologic piercing points and some tectonic implications. *Geology*, 31, 335-338.

Reid, A., Hand, M., Jagodzinski, E., Kelsey, D., Pearson, N., 2008. Paleoproterozoic orogenesis in the southeastern Gawler Craton, South Australia. *Australian Journal of Earth Sciences*, 55, 449–471.

Rignot, E., Mouginot, J., Scheuchl, B., 2011. Ice flow of the Antarctic ice sheet. *Science*, 333, 1427-1430; doi:10.1126/science.1208336.

Rose, K.C., Ferraccioli, F., Jamieson, S.S.R., Bell, R.E., Corr, H., Creyts, T.T., Braaten, D., Jordan, T.A., Fretwell, P.T., Damaske, D., 2013. Early East Antarctic Ice Sheet growth recorded in the landscape of the Gamburtsev Subglacial Mountains. *Earth and Planetary Science Letters*, 375, 1-12; doi:10.1016/j.epsl.2013.03.053.

Ross, G.M., Villeneuve, M., 2003. Provenance of the Mesoproterozoic (1.45 Ga) Belt Basin (western North America): Another piece in the pre-Rodinia paleogeographic puzzle. *Geological Society of America Bulletin*, 115, 1191–1217, doi: 10.1130/B25209.1.

Sambridge, M.S., Compston, W., 1994. Mixture modeling of multi-component data sets with application to ion-probe zircon ages. *Earth and Planetary Science Letters*, 128, 373-390.

Scherer, E.E., Whitehouse, M.J., Munker, C., 2007. Zircon as a monitor of crustal growth. *Elements*, 3, 19-24.

Schroeder, D.M., Blankenship, D.D., Young, D.A., Quartini, E., 2014. Evidence for elevated and spatially variable geothermal flux beneath the West Antarctic Ice Sheet. *Proceedings of the National Academy of Sciences*, 111(25), 9070–9072.

Söderlund, U., Patchett, P.J., Vervoort, J.D., Isachsen, C.E., 2004. The ^{176}Lu decay constant determined by Lu-Hf and U-Pb isotope systematics of Precambrian mafic intrusions. *Earth and Planetary Science Letters*, 219(3–4), 311-324, doi.org/10.1016/S0012-821X(04)00012-3.

Stearns, L.A., Smith, B.E., Hamilton, G.S., 2008. Increased flow speed on a large East Antarctic outlet glacier caused by subglacial floods. *Nature Geoscience*, 1, 827-831.

Steiger, R.H., Jäger, E., 1977. Subcommission on geochronology: convention on the use of decay constants in geo- and cosmochronology. *Earth and Planetary Science Letters*, 36, 359–362.

Stewart, E.D., Link, P.K., Fanning, C.M., Frost, C.D., McCurry, M., 2010. Paleogeographic implications of non–North American sediment in the Mesoproterozoic upper Belt Supergroup and Lemhi Group, Idaho and Montana, USA. *Geology*, 38, 927-930, doi: 10.1130/G31194.1.

Tera, F., Wasserburg, G., 1972. U-Th-Pb systematics in three Apollo 14 basalts and the problem of initial Pb in lunar rocks. *Earth and Planetary Science Letters*, 14, 281-304.

Thorkelson, D.J., Laughton, J.R., 2016. Paleoproterozoic closure of an Australia–Laurentia seaway revealed by megaclasts of an obducted volcanic arc in Yukon, Canada. *Gondwana Research*, 33, 115-133.

Thorkelson, D.J., Mortensen, J.K., Creaser, R.A., Davidson, G.J., Abbott, J.G., 2001a. Early Proterozoic magmatism in Yukon, Canada: constraints on the evolution of northwestern Laurentia. *Canadian Journal of Earth Sciences,* 38, 1479–1494.

Thorkelson, D.J., Mortensen, J.K., Davidson, G.J., Creaser, R.A., Perez, W.A., Abbott, J.G., 2001b. Early Mesoproterozoic intrusive breccias in Yukon, Canada: the role of hydrothermal systems in reconstructions of North America and Australia. *Precambrian Research*, 111, 31–55.

Valley, J.W., 2003. Oxygen isotopes in zircon: *in* Hanchar, J.M., and Hoskin, P.W.O. (Eds.), *Zircon*, Reviews in Mineralogy and Geochemistry: Washington, DC, Mineralogical Society of America, 343-385.

Valley, J.W., Kinny, P.D., Schulze, D.J., Spicuzza, M.J., 1998. Zircon megacrysts from kimberlite: oxygen-isotope variability among mantle melts. *Contributions to Mineralogy and Petrology*, 133, 1–11.

van de Flierdt, T., Hemming, S.R., Goldstein, S.L., Gehrels, G.E., Cox, S.E., 2008. Evidence against a young volcanic origin of the Gamburtsev Subglacial Mountains, Antarctica. *Geophysical Research Letters*, 35, L21303.

Van Liefferinge, B., and Pattyn F., 2013, Using ice-flow models to evaluate potential sites of million

year-old ice in Antarctica. *Climates Past*, 9, 2335–2345, doi:10.5194/cp-9-2335-2013.

Van Schmus, W.R., Bickford, M.E., Condie, K.C., 1993. Early Proterozoic crustal evolution. In: Reed, J.C., Jr., ed., *Precambrian: Conterminous U.S. Geology of North America*, C-2, Geological Society of America, Boulder, Colorado, pp. 270–281.

Vervoort, J.D., Kemp, A.I.S., Fisher, C., Bauer, A., 2015. The rock record has it about right—no significant continental crust formation prior to 3.8 Ga. American Geophysical Union, Fall Meeting Abstracts, San Francisco, California.

Vervoort, J.D., Kemp, A., Fisher, C., and Bauer, A., 2016a. Development of the depleted mantle reservoir and growth of the continental crust begins at ~ 3.8 Ga. 35th International Geologic Conference, Cape Town, South Africa.

Vervoort, J.D., Lewis, R.S., Fisher, C., Gashnig, R.M., Jansen, A.C., Brewer, R., 2016b. Neoarchean and Paleoproterozoic crystalline basement rocks of north-central Idaho: constraints on the formation of western Laurentia. *Geological Society of America Bulletin*, 128, 94-109.

Vervoort, J.D., Plank, T., Prytulak, J., 2011. The Hf–Nd isotopic composition of marine sediments. *Geochimica et Cosmochimica Acta*, 75, 5903–5926.

Wang, D., Vervoort, J.D, Fisher, C.M., Lewis, R.S., Buddington, A.M., Doughty, P.T., 2014. The basement terranes of north central Idaho: Filling in the gap between the Priest River and Clearwater complexes. *Geological Society of America Abstracts with Programs*, 46(5), 33.

Whillans, I.M., Cassidy, W.A., 1983. Catch a falling star: Meteorites and old ice. *Science*, 222, 55-57.

White, W.M., Klein, E.M., 2014. Composition of the oceanic crust. In *Treatise on Geochemistry*, 2nd Ed., Elsevier, 457-496, doi: 10.1016/B978-0-08-095975-7.00315-6.

Whitmeyer, S.J., Karlstrom, K.E., 2007. Tectonic model for the Proterozoic growth of North America. *Geosphere*, 3, 220-259.

Wooden, J.L., Barth, A.P., Mueller, P.A., 2013. Crustal growth and tectonic evolution of the Mojave crustal province: insights from hafnium isotope systematics in zircons. *Lithosphere*, 5, 17–28.

Wörner, G., Moorbath, S., Horn, S., Entenmann, J., Harmon, R.S., Davidson, J., López-Escobar, L., 1994.

Large- and fine-scale geochemical variations along the Andean arc of northern Chile (17. 5°–22°S). *In* Reutter, K.J., Scheuber, E., and Wigger, P.J. (Eds.), *Tectonics of the Southern Central Andes: Structural Evolution of an Active Continental Margin*, Springer-Verlag, Berlin, 77–9.

Zhao, G.C., Sun, M., Wilde, S.A., Li, S.Z., 2004. A Paleo-Mesoproterozoic supercontinent: assembly, growth and breakup. *Earth-Science Reviews*, 67, 91–123.

Zirakparvar, N., Vervoort, J., Lewis, R., McClelland, W., 2010. Insights into the thermal evolution of the Belt-Purcell Basin; evidence from Lu-Hf garnet geochronology. *Canadian Journal of Earth Sciences*, 47, 161-179.

Figure captions:

Fig. 1. Maps showing major ice streams and subglacial bed relief of central East Antarctica. (a) Ice velocity of major catchments (Rignot et al., 2011). (b) Subglacial bed relief from Bedmap2 data (Fretwell et al., 2013). Inset in (b) shows area of coverage in Antarctica. Solid white lines mark major drainage divides. Main sample sites shown by white dots. Outlet glaciers: Bd, Beardmore; By, Byrd; Ni, Nimrod; Sc, Scott; Sh, Shackleton. Other geographic features: ASB, Aurora Subglacial Basin; GM, Grove Mountains; GSM, Gamburtsev Subglacial Mountains; LT, Lambert Trough; LV, Lake Vostok; MR, Miller Range; PCM, Prince Charles Mountains; PM, Pensacola Mountains; QER, Queen Elizabeth Range; QMM, Queen Maud Mountains; RI, Ross Island; SVL, Southern Victoria Land; TM, Thiel Mountains; WSB, Wilkes Subglacial Basin.

Fig. 2. Map of the Transantarctic Mountains region of Antarctica, showing field sites where glacial moraines were visited and sampled. White circles indicate sites where samples for this study were

collected. Sample information listed in Table 1. Base image from MODIS radiometer Mosaic of Antarctica (Haran et al., 2005, 2013).

Fig. 3. Photos of example field occurrences where igneous clasts were collected from glacial moraines. (a) Sample site at Lonewolf Nunataks along southern edge of Byrd Glacier. (b) Clast at Argo Glacier site showing round shape and glacial striations. Pencil is about 14 cm long. Sample petrographic characteristics are listed in Supplementary Data Table 1 and representative hand-sample photographs and thin section photomicrographs are provided in Appendix 1.

Fig. 4. Geochemical discrimination plots of igneous clast compositions (data listed in Supplementary Data Table 2). (a) and (b) Granite major-element indices plotted versus SiO_2, after Frost et al. (2001). FeO* is total iron. MALI (modified alkali-lime index) = $Na_2O + K_2O - CaO$. (c) and (d) Granite trace-element tectonic discrimination diagrams from Pearce et al. (1984). Abbreviations: ORG, orogenic granites; syn-COLG, syn-collisional granites; VAG, volcanic-arc granites; WPG, within-plate granites. Compositions of ca. 1.45 Ga Mt-series and peraluminous two-mica granites found in Laurentia shown in (a) for comparison (Anderson and Cullers, 1999; Anderson and Morrison, 2004). Compositions of ca. 1.59 Ga Gawler Range Volcanics (GRV) in Australia and moraine samples from Terre Adélie Craton (TAC) shown in (a) and (c) for comparison (Peucat et al., 2002).

Fig. 5. Rare-earth and trace-element plots of igneous clasts, grouped by age (data listed in Supplementary Data Table 2). (a) Rare-earth element distributions plotted relative to chondrites (reference average CI chondrite composition from Lodders et al., 2009). (b) Trace-element spider diagram plotted relative to average MORB (reference log-normal mean MORB composition from White and Klein, 2014).

Fig. 6. U-Pb results for samples with ages of about 1200 Ma, including Concordia plots of all data and inset age histograms with relative probability distributions. Sample information, characteristics and representative zircon CL images provided in Appendix 1; data listed in Supplementary Data Tables 3-4. Generally, the Concordia plots and probability densities show the same analyses, but the probability plots show only those analyses clustering around the magmatic age whereas the corresponding Concordia plot may show more (or all) analyses; in a few cases some of the most highly discordant analyses that do not contribute to the age determination are not shown. Ellipses of individual analyses plotted with 1σ uncertainty. (a) Sample 10LWA-13.1, a Ms-Bt granite from Lonewolf Nunataks (14 of 21 analyses shown). (b) Sample 10LWA-11.1, a porphyritic red Bt granite from Lonewolf Nunataks (17 of 18 analyses shown).

Fig. 7. U-Pb results for samples with ages between about 1400-1500 Ma. Data plotted as in Figure 6 and listed in Supplementary Data Tables 5-14. Individual analyses showing anomalous behavior due to greater uncertainty, strong reverse discordance, or departure from the main Pb-loss trend (unfilled ellipses) were not included in age regressions. (a) Sample 10MSA-2.3, a red Bt leucogranite from Mt. Sirius (16 of 18 analyses shown). (b) Sample 10LWA-6.5, a red Ms-Bt granite from Lonewolf Nunataks (15 of 15 analyses shown; analyses shown by unfilled ellipses not included in determination of intercept age). (c) Sample 10TNA-1.1, a rapikivi Bt granite from Turret Nunatak (4 of 4 analyses shown). (d) Sample 10LWB-4.3, a mylonitic Grt-Bt granite orthogneiss from Lonewolf Nunataks (16 of 16 analyses shown). (e) Sample 10LWA-6.6, a foliated, annealed pink Bt granite from Lonewolf Nunataks (15 of 15 analyses shown; analyses shown by unfilled ellipses not included in determination of intercept age). (f) Sample 10LWA-9.2, a mylonitic grey Bt granite from Lonewolf Nunataks (12 of 12 analyses shown). (g) Sample 10LWA-9.3, a porphyritic grey Bt granite from Lonewolf Nunataks (11 of 13 analyses shown). (h) Sample 10LWB-3.8, a grey Bt granite porphyry from Lonewolf Nunataks (14 of 18 analyses shown). (i) Sample 10LWA-20.1, a Bt granite porphyry from Lonewolf Nunataks (12 of 12 analyses shown). (j)

Sample 10MSA-3.5, a foliated Ms-Bt leucogranite from Mt. Sirius (20 of 21 analyses shown). Rims with Grenvillian ages shown in green.

Fig. 8. U-Pb results for sample 10LWA-6.4, a foliated red Ms-Bt granite from Lonewolf Nunataks, with an age of about 1570 Ma. Data plotted as in Figure 6 and listed in Supplementary Data Table 15. Individual analyses showing anomalous behavior due to Pb loss (unfilled ellipses) were not included in age regressions or weighted mean calculations.

Fig. 9. U-Pb results for samples with ages of about 1790 Ma. Data plotted as in Figure 6 and listed in Supplementary Data Tables 16-17. (a) Sample 10LWA-14.1, a red veined Bt granite from Lonewolf Nunataks. (b) Sample 10MRA-2.1, a Grt-Bt granite from Milan Ridge, Miller Range. Six analyses from overgrowths are shown only on the age probability distribution (inset, green).

Fig. 10. U-Pb results for samples with ages of about 1850 Ma. Data plotted as in Figure 6 and listed in Supplementary Data Tables 18-22. (a) Sample 10LWB-4.5, a foliated red Bt granite from Lonewolf Nunataks. (b) Sample 10LWA-6.3, a layered Bt granite from Lonewolf Nunataks. (c) Sample 10LWA-7.1, a mylonitic Hbl-Bt granodiorite from Lonewolf Nunataks. (d) Sample 10LWB-4.1, a foliated porphyritic red Bt granite from Lonewolf Nunataks. (e) Sample 10MSA-3.3, a foliated Bt granite from Mt. Sirius. Seven analyses from overgrowths are shown only on the age probability distribution (inset, green).

Fig. 11. U-Pb results for samples with ages of about 2010 Ma. Data plotted as in Figure 6 and listed in Supplementary Data Tables 23-24. (a) Sample 10LWA-10.1, a foliated Hbl-Bt granite from Lonewolf Nunataks. (b) Sample 10LWA-8.1, a foliated Hbl-Bt granodiorite from Lonewolf Nunataks. One

individual analysis showing anomalous behavior and departure from the main Pb-loss trend (unfilled ellipse) was not included in age regressions.

Fig. 12. Summary of interpreted U-Pb zircon crystallization ages for glacial igneous clasts compared to other known geologic events. Sources of clast age data: Goodge et al. (2008, 2010, 2012); this study. Age range of Grenvillian metamorphic reworking (1200-1130 Ma) as documented in this paper shown by vertical green band. Ages of pre-Ross igneous and high-grade metamorphic events recognized in crystalline basement to the central Transantarctic Mountains (Nimrod Group) from Goodge and Fanning (1999), Goodge et al. (2001, 2016).

Fig. 13. $\delta^{18}O$ compositions versus crystallization age for zircon from igneous glacial clasts. Each symbol represents the arithmetic mean O-isotopic composition at a measured age, as summarized in Table 2. Individual sample data listed in Supplementary Data Table 25. Error bars are 2σ external errors for O-isotope measurements and 2σ for U-Pb ages. All individual O-isotope spot analyses are shown by small grey dots. Average mantle zircon isotopic composition from Valley et al. (1998) and Valley (2003).

Fig. 14. (a) Epsilon Hf versus crystallization age for zircon from igneous glacial clasts. Each symbol represents the weighted-mean Hf isotopic composition at a measured age, as summarized in Table 3. Error bars are 2SE for Hf-isotope measurements and 2σ for U-Pb ages. All individual Hf-isotope spot analyses are shown by small grey dots. Depleted-mantle evolution model assumes $\varepsilon_{Hf} = 0$ until 3.8 Ga, after which it evolves with a $^{176}Lu/^{177}Hf = 0.0398$ to a present-day value of +16 (Vervoort et al., in prep). Diagonal dashed lines show a two-stage isotopic evolution assuming a first stage $^{176}Lu/^{177}Hf$ of 0.0125 for the precursor crust (Chauvel et al., 2014). (b) Epsilon Hf model illustrating the six age groups discussed in the text. Crustal evolution trends (pink) assume a $^{176}Lu/^{177}Hf$ of 0.0125. Four different periods of both

magmatic activity and crustal growth in East Antarctica (in light blue at ~1500, ~1850, ~2300 and ~2700 Ma) are suggested from the Hf-isotope data of igneous glacial clasts. See text for discussion.

Fig. 15. Hf- versus O-isotope compositions for igneous glacial clasts. Uncertainties as plotted in figures 13 and 14.

Fig. 16. Map summarizing igneous clast ages from glacial sample sites discussed in this paper, plus one additional site at Kon-Tiki Nunatak (Goodge et al., 2010, 2012). Red hachured line marks edge of the Neoproterozoic rifted cratonic margin of East Antarctica, and transparent shaded regions outline likely crustal provinces, all defined by aeromagnetic and gravity data (Goodge and Finn, 2010). Nimrod Group basement complex (pink) defined by outcrop in the Miller (MR) and Geologists (GR) ranges, along with subglacial geologic terrain marked by similar aeromagnetic anomalies. Nimrod igneous province (brown) is likewise defined by high-amplitude, positive subglacial magnetic anomalies that resemble Proterozoic crustal provinces in Laurentia and Australia (Daly et al., 1998; Finn and Sims, 2005; Goodge and Finn, 2010). Base image is from MODIS radiometer data, as in Fig. 2. Glacial till sites sampled for detrital zircon geochronology shown by yellow stars (Goodge et al., 2010).

Fig. 17. Comparison of (a) igneous glacial clast ages (magenta line, this study) with ages from (b) composite detrital zircon populations in Neoproterozoic rift-margin successions (orange line, Beardmore Group; Goodge et al., 2002, 2004) and (c) composite detrital zircon populations in metamorphic basement metasedimentary rocks (purple line, Argosy Schist; Goodge and Fanning, 2016). Ages of metamorphism inferred to have caused episodic Pb-loss in the source area for the glacial clasts shown by dark green bar in (a). Also shown are principal ages known from Nimrod Complex metamorphic basement assemblage (light purple bars, Goodge and Fanning, 2016). Glacial clast age groups shown for reference by vertical

dashed lines in magenta. Also shown for reference are ages of Grenville Province (light green) and ~1.4 Ga granite province in North America (light red).

Fig. 18. Map showing potential source areas for the glacial igneous clasts discussed in this paper. Principal features are ice-sheet catchment areas (marked by blue drainage divides), ice flow directions (arrows), subglacial highland and lowland areas (tan and light blue, respectively), and areas of rock outcrop and Precambrian basement exposure, simplified from Fig. 1. Composite source area for the five sample localities (outlined in heavy black line) was determined from the ice flow-fields that contribute ice to each of the sample sites. Because transport distance is not known for any of the individual clasts, possible bedrock sources could reside anywhere between the sample sites and the top of the ice catchment overlapping the Gamburtsev Subglacial Mountains.

Fig. 19. Comparison of Hf-isotope compositions between East Antarctic glacial clasts and representative basement complexes in the Gawler craton, Australia, and western Laurentia. Sources of data include: Goodge and Vervoort (2006); Fanning et al. (2007); Hand et al. (2007); Reid et al. (2008); Howard et al. (2011); Belousova et al. (2009); Wooden et al. (2013); Ramo et al. (2003); Fisher et al. (2013, 2014).

Fig. 20. Reconstruction showing correlations of crustal provinces in East Antarctica, Australia and Laurentia at about 1.1 Ga. Source region of glacial clasts (light blue) as shown in Figure 18. Ages of clasts from this source region highlighted by stars (Goodge et al., 2008, 2010; this study). Geological provinces in East Antarctica, Australia and Laurentia whose principal ages correlate with the clast populations are shown by half-filled circles; provinces with both age and Hf-isotope correspondence shown by filled circles. Base reconstruction after Goodge et al. (2008). Extent of Mawson Continent after Goodge and Fanning (2016). Abbreviations: GC, Gawler Craton; GSM, Gamburtsev Subglacial

Mountains; IS, Isan Supergroup; MP, Mojave Province; NC, Nimrod Complex; NI, northern Idaho (Clearwater Complex, Laclede gneiss); NIP, Nimrod igneous province; SPCM, southern Prince Charles Mountains; SR, Shackleton Range; TA, Terre Adélie; WS, Wernicke Supergroup (Yukon). Position of 1.45-1.30 Ga Rocky Cape Group (RCG) siliciclastic sediments in Tasmania reconstructed to position between potential sources in East Antarctica and Laurentia (Mulder et al., 2015). Additional Laurentian age correlations shown for 1.0-1.3 Ga magmatism and metamorphism (Parrish and Reichenbach, 1991; Doughty and Chamberlain, 2008; Zirakparvar et al., 2010; Milidragovic et al., 2011) and ~1.6 Ga igneous activity (Doughty et al., 1998), in Yukon associated with IOCG mineral deposits (Thorkelson et al., 2001; Furlanetto et al., 2016). This reconstruction shows the key linkages between East Antarctica, Australia and Laurentia at the specific times shown by the sample ages; it is not meant to imply that there is no inter-cratonic mobility between about 2.0-1.0 Ga.

Fig. 21. Comparison of major orogenic, sedimentation and magmatic events in East Antarctica, Australia, and western Laurentia. Ages of igneous glacial clasts from this study shown by circles as in Figure 20; inferred presence of East Antarctic crust with these ages shown by circles with dashed outlines. Cratonic elements >2 Ga shown in pink. Correlations based on both age and Hf-isotope compositions shown by magenta lines (see Fig. 20 for references). Inferred sedimentary provenance links shown by blue arrows. Tectonic activity associated with assembly of the Columbia-Nuna and Rodinia supercontinents (at ~1.8 and ~1.1 Ga, respectively) shown in light brown. Named geologic units and events are representative or indicative of a given age and not meant to be comprehensive. Ties between discrete igneous and metamorphic ages, isotopic compositions of distinctive igneous events, sedimentary provenance linkages, and general stratigraphic and orogenic pattern indicate that these three cratonic elements shared a common geotectonic history between about 2.0-1.0 Ga, including alternating periods of crustal extension and arc-related convergence, that reflects a long-lived association. References include: (a) East Antarctic glacial clasts (Goodge et al., 2008, 2010; this study); (b) East Antarctic crust (Goodge et al., 2001;

Goodge and Fanning, 2016); (c) western Australia (Betts, 2002); (d) central Australia (Betts and Giles, 2006; Fanning et al., 2007; Hand et al., 2007; Berry et al., 2008; Betts et al., 2008); (d) northern Laurentia (Thorkelson et al., 2001, 2016; Milidragovic et al., 2001; Furlanetto et al., 2016); (e) southern Laurentia (Doughty et al., 1998; Goodge and Vervoort, 2006; Whitmeyer and Karlstrom, 2007; Zirakparvar et al., 2010; Vervoort et al., 2016); (f) sedimentary provenance linkages (Fanning, 2003; Ross and Villeneuve, 2003; Goodge et al., 2004; Link et al., 2007; Stewart et al., 2010; Daniel et al., 2013; Medig et al., 2014; Mulder et al., 2015; Furlanetto et al., 2016).

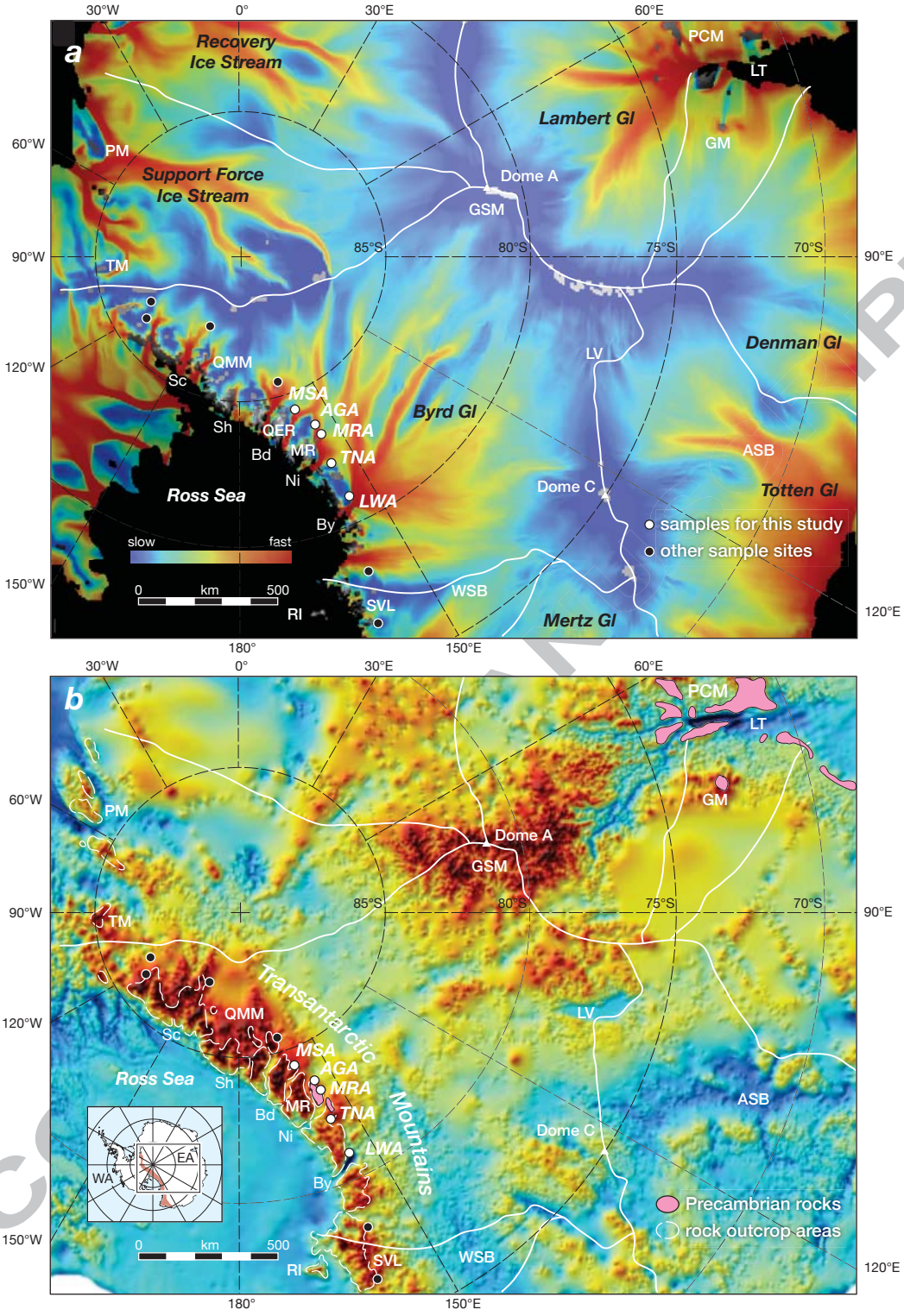

Goodge et al. [Fig.1]

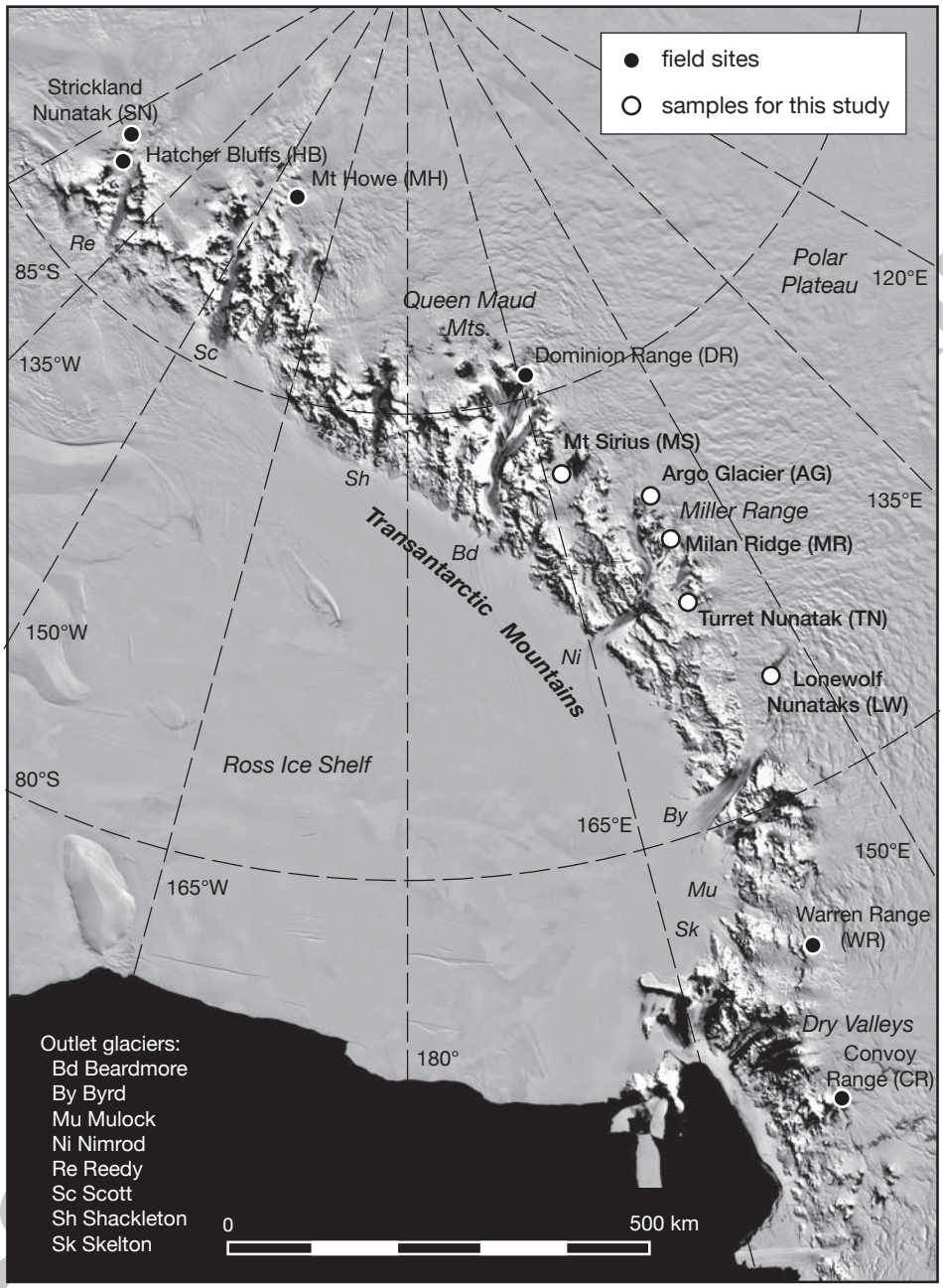

Goodge et al. [Fig. 2]

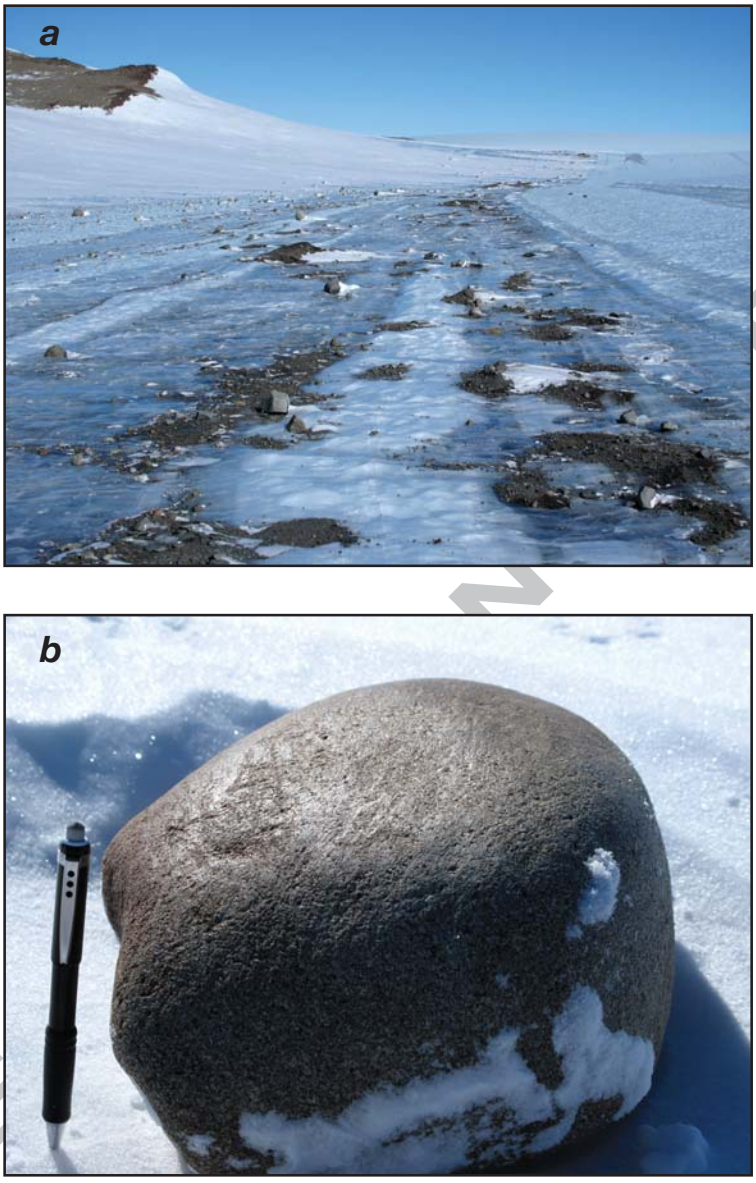

Goodge et al. [Fig. 3]

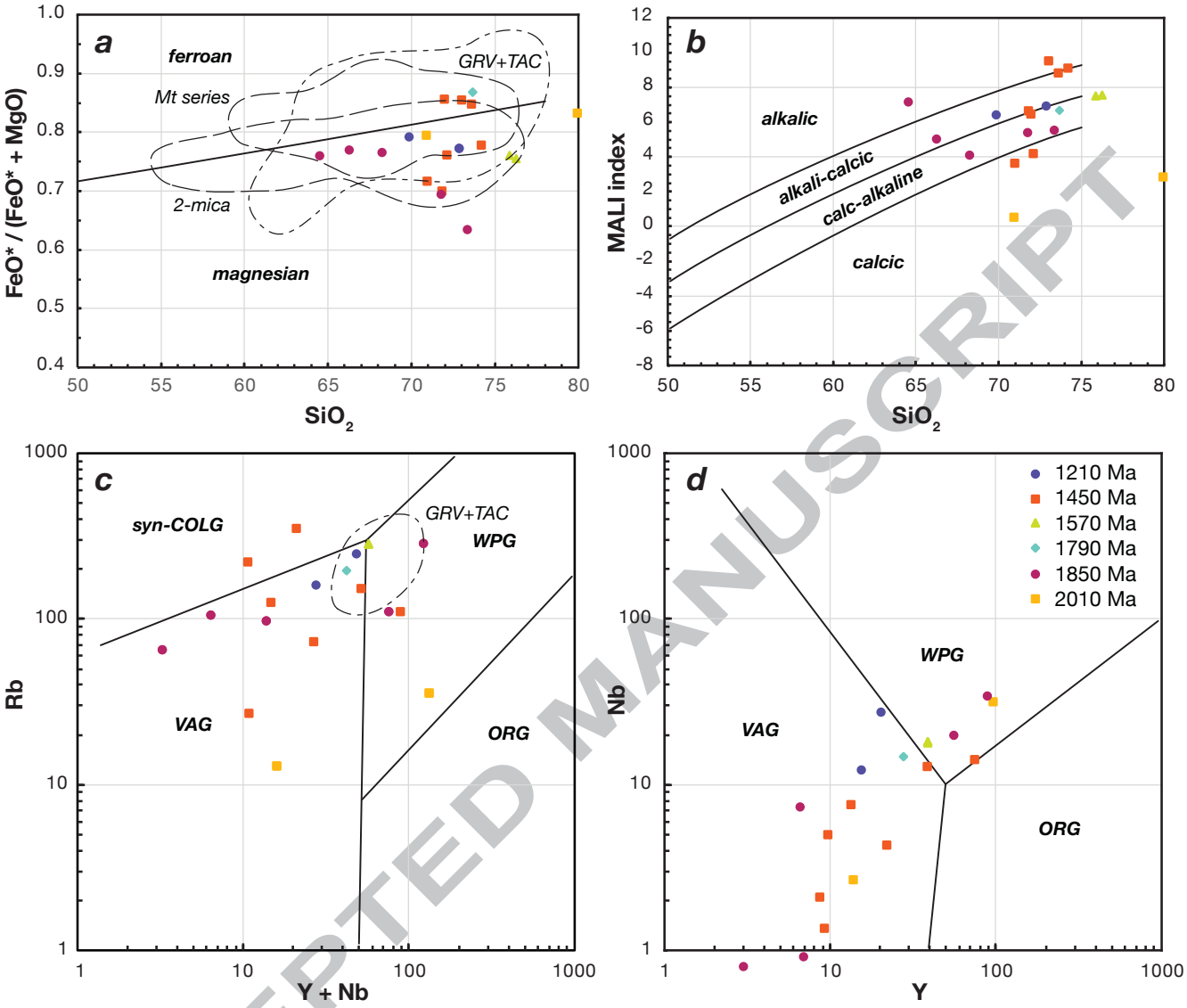

Goodge et al. [Fig. 4]

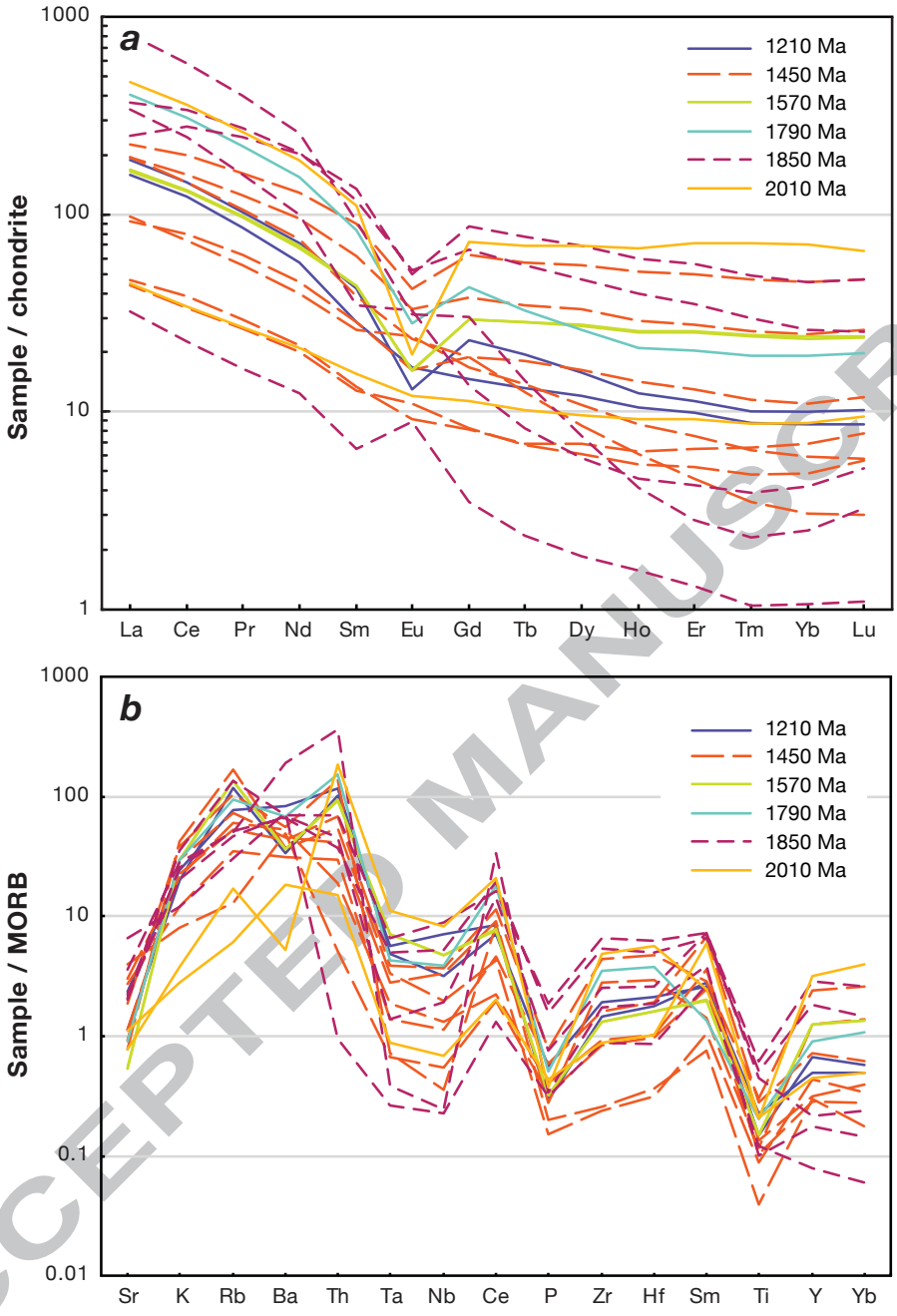

Goodge et al. [Fig. 5]

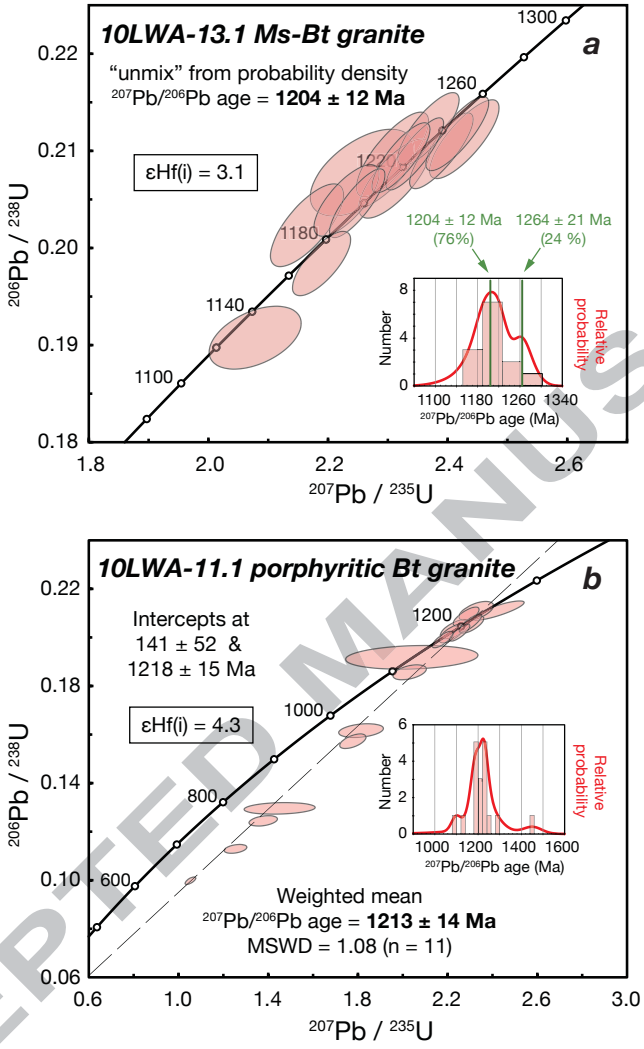

Goodge et al. [Fig. 6]

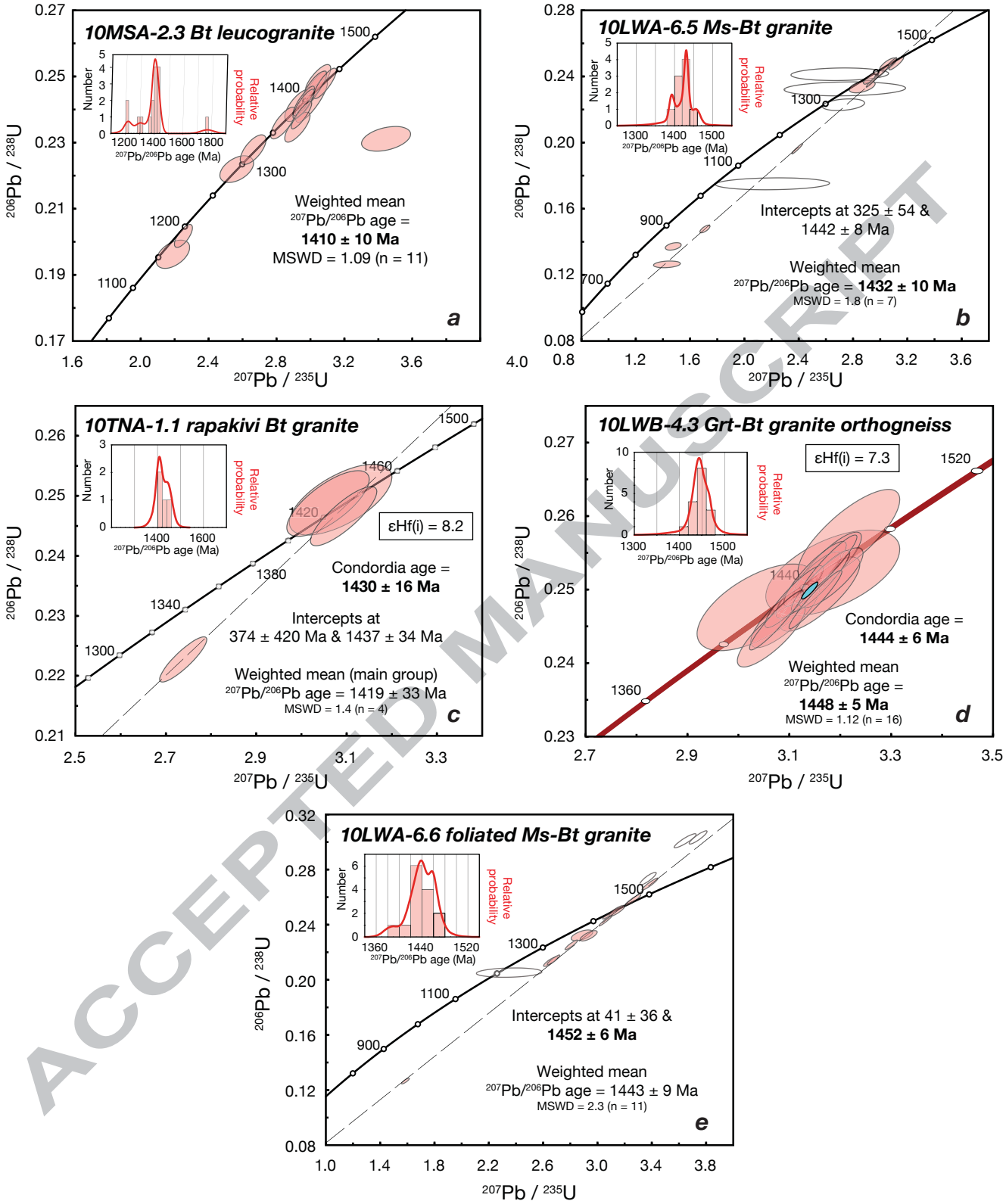

Goodge et al. [Fig. 7A]

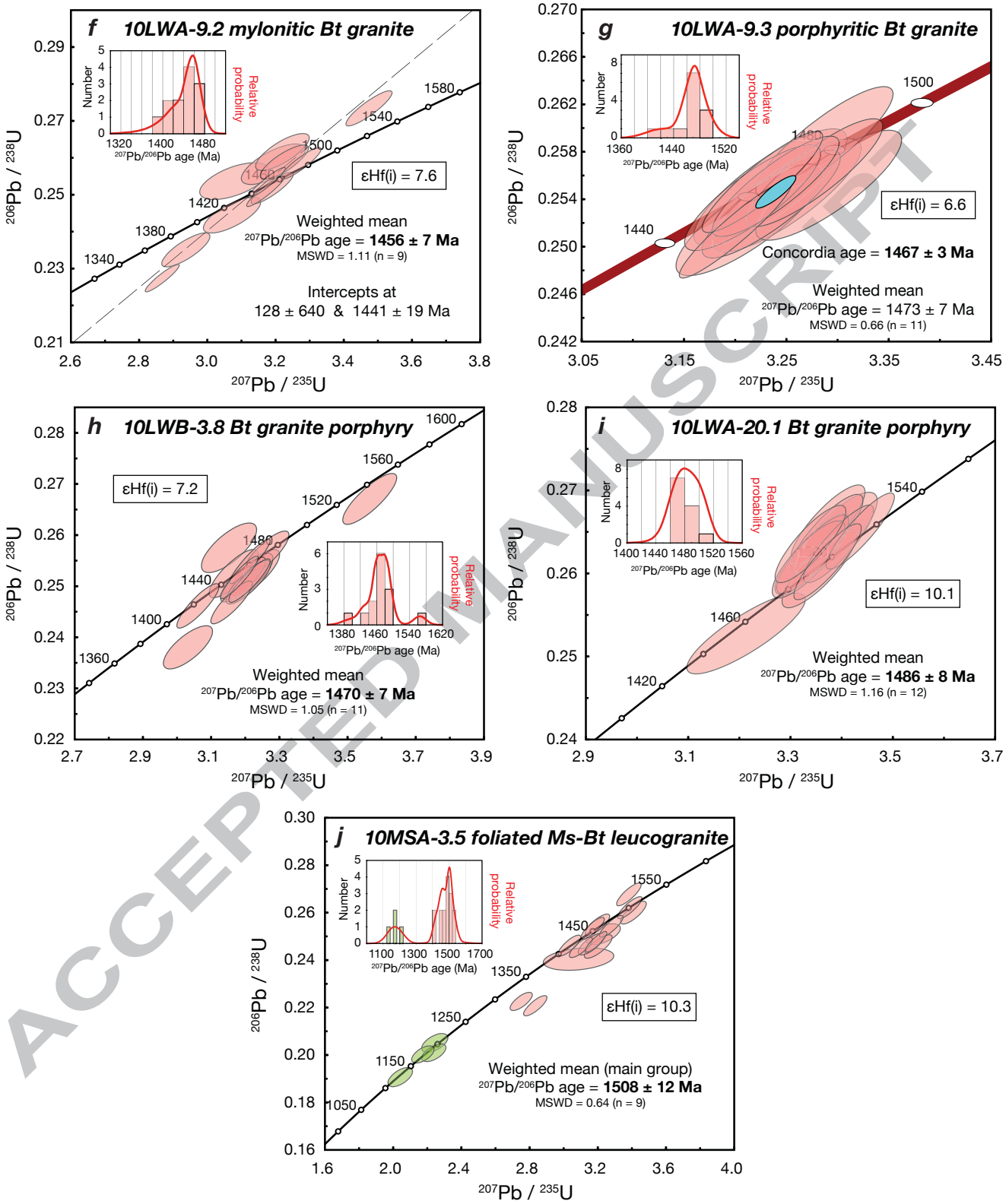

Goodge et al. [Fig. 7B]

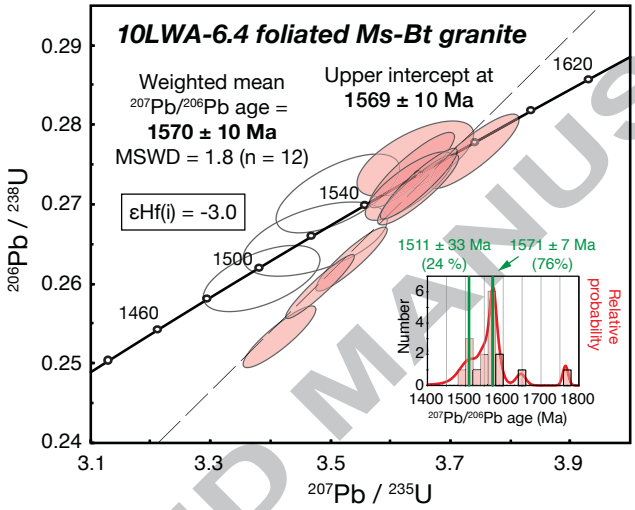

Goodge et al. [Fig. 8]

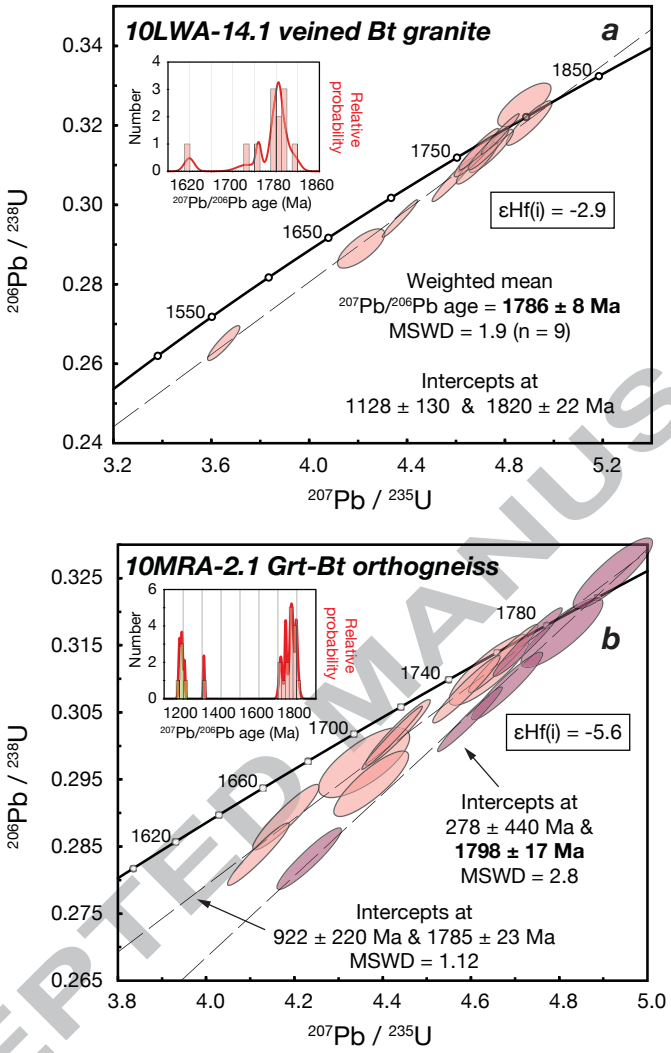

Goodge et al. [Fig. 9]

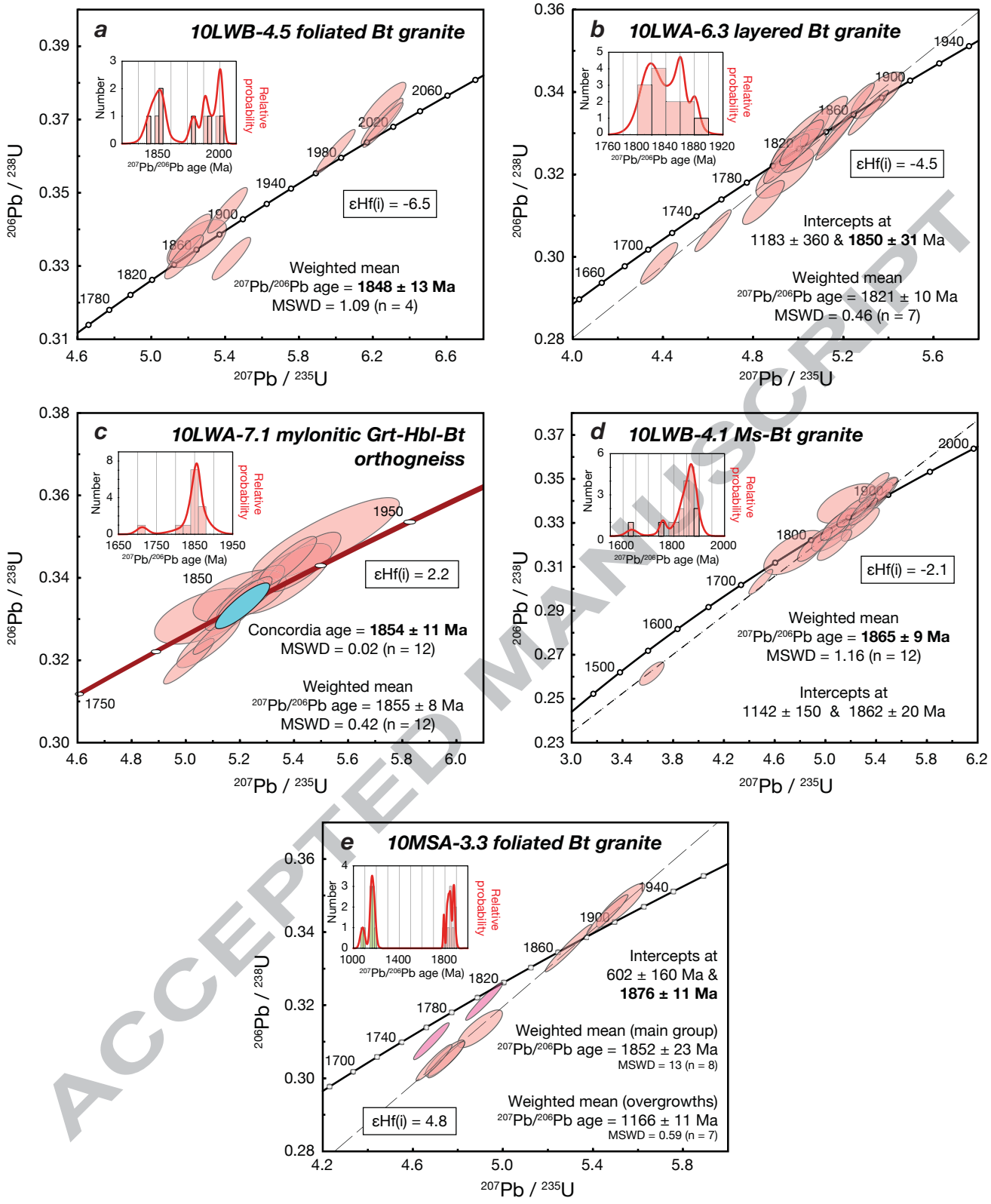

Goodge et al. [Fig. 10]

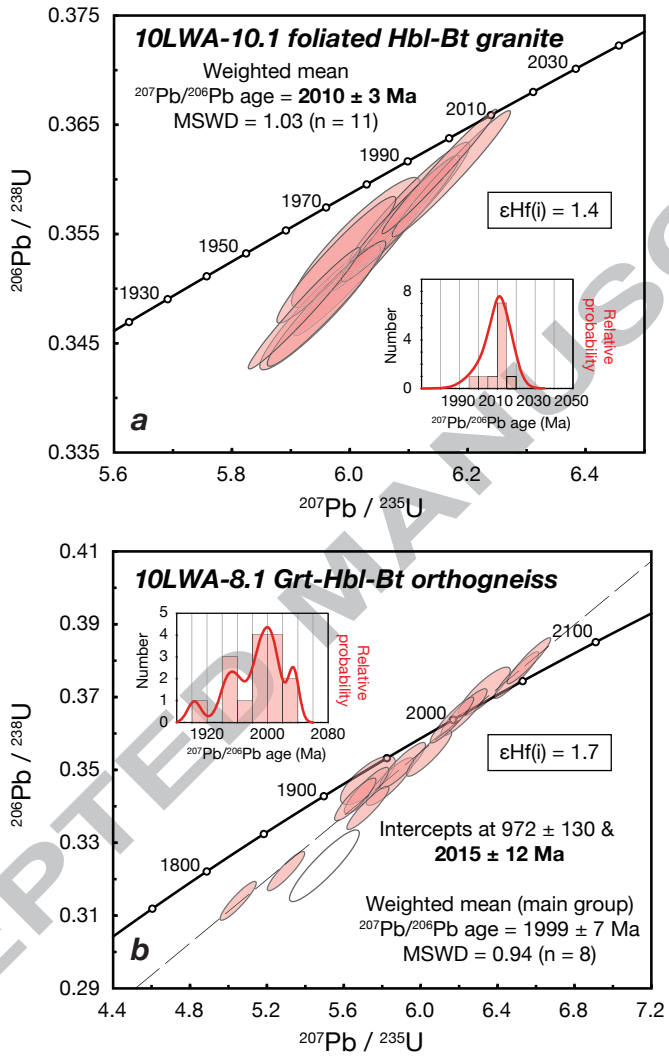

Goodge et al. [Fig. 11]

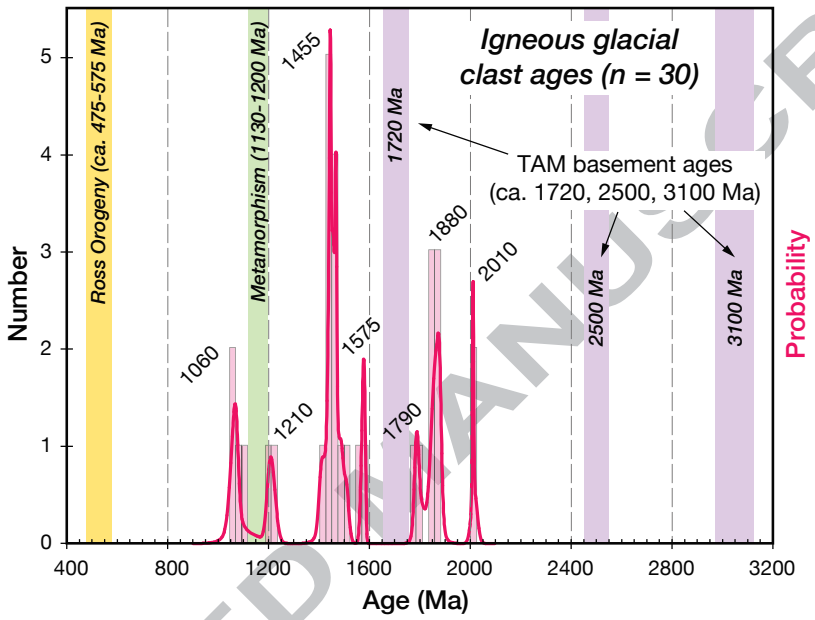

Goodge et al. [Fig. 12]

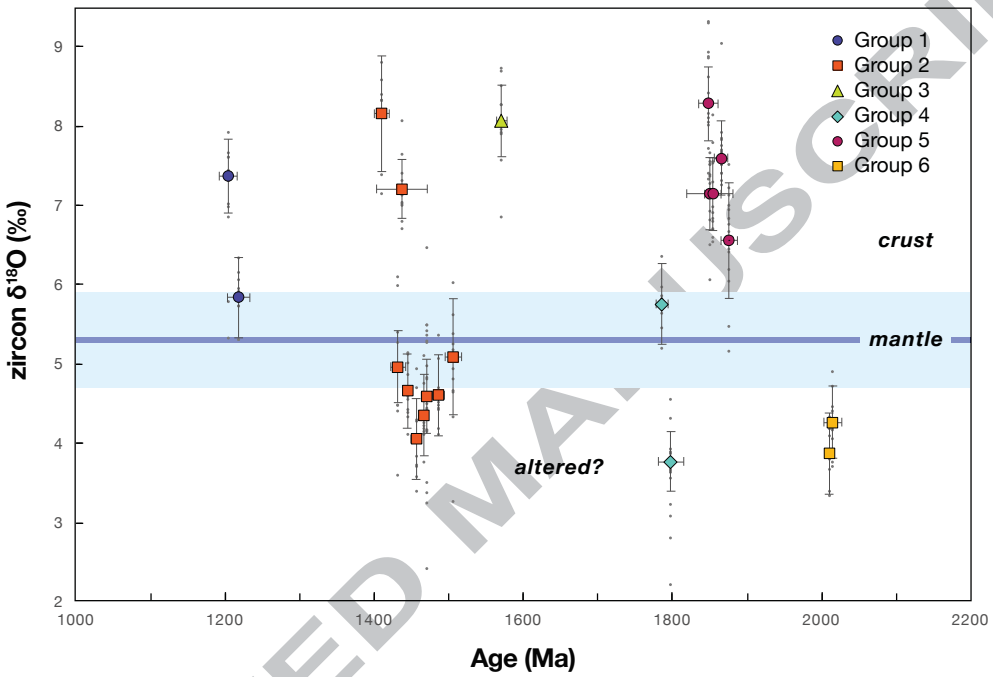

Goodge et al. [Fig. 13]

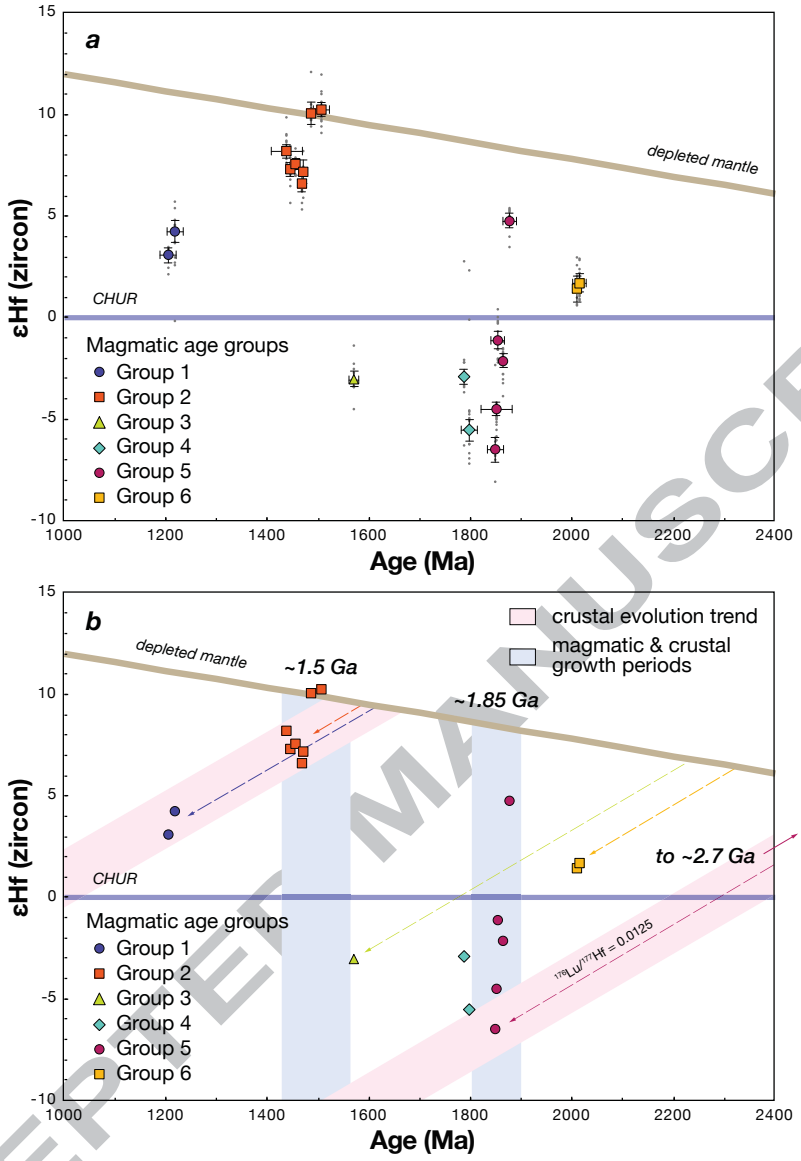

Goodge et al. [Fig. 14]

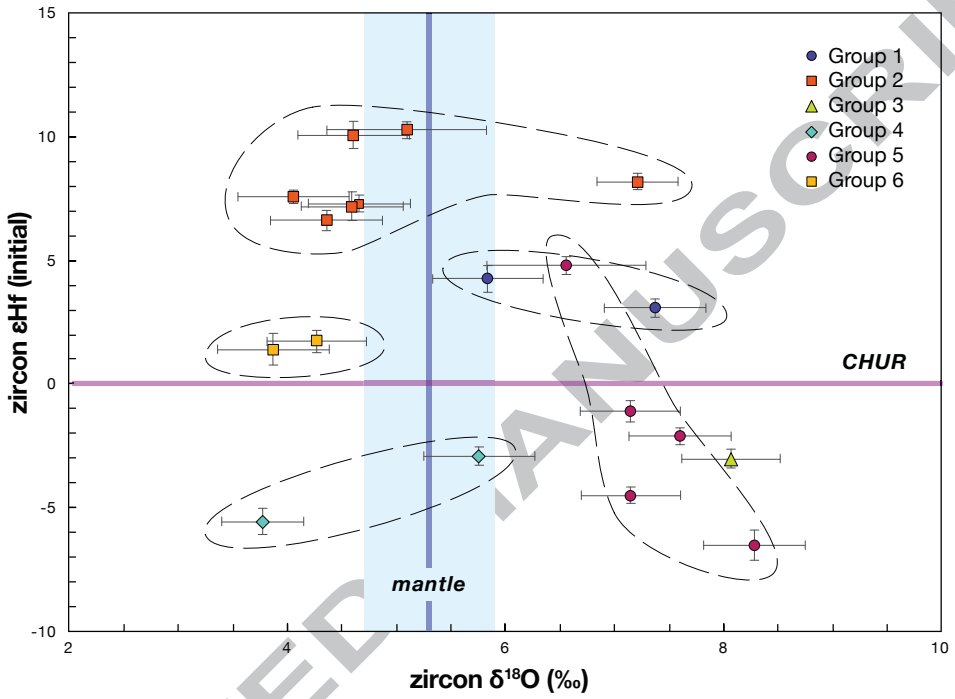

Goodge et al. [Fig. 15]

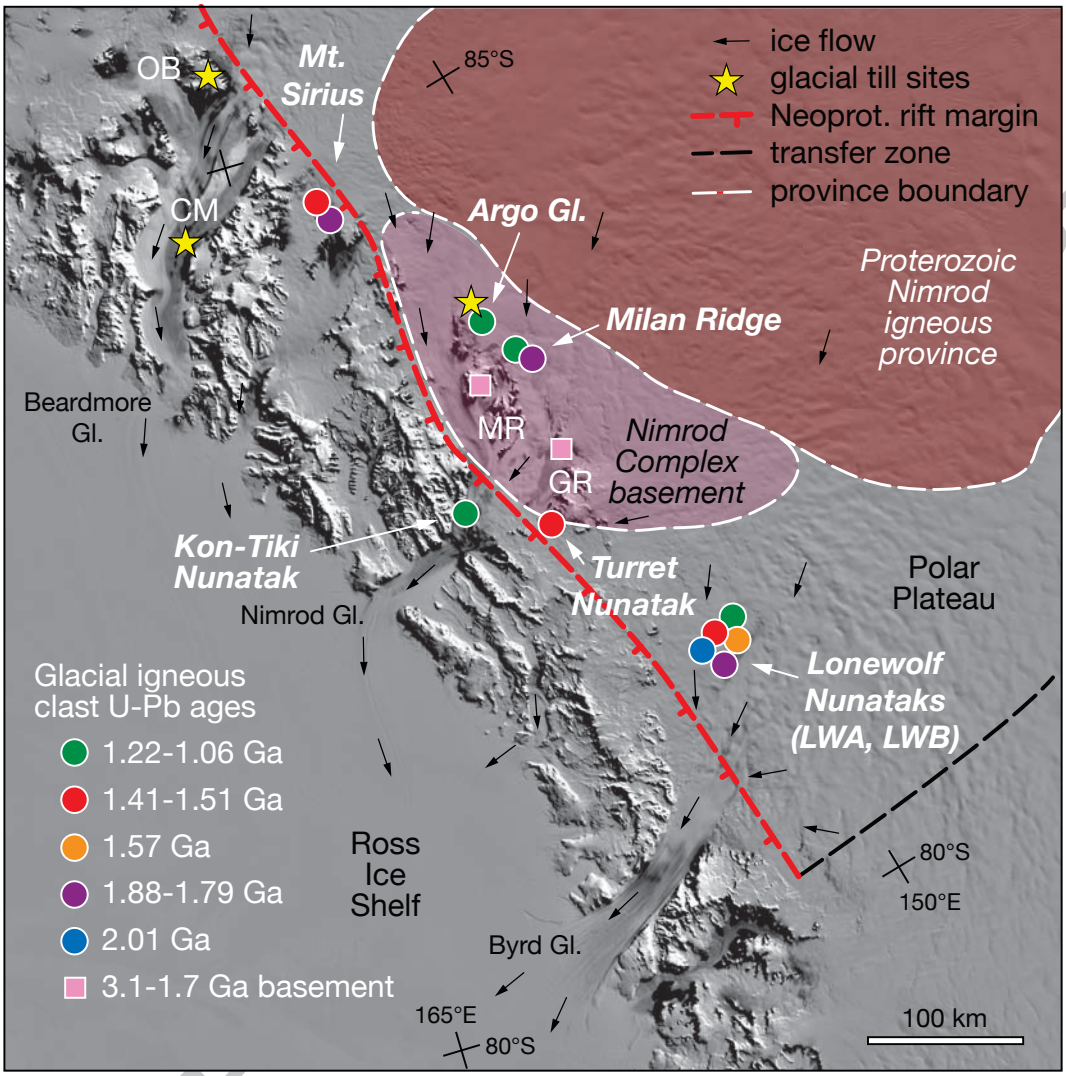

Goodge et al. [Fig. 16]

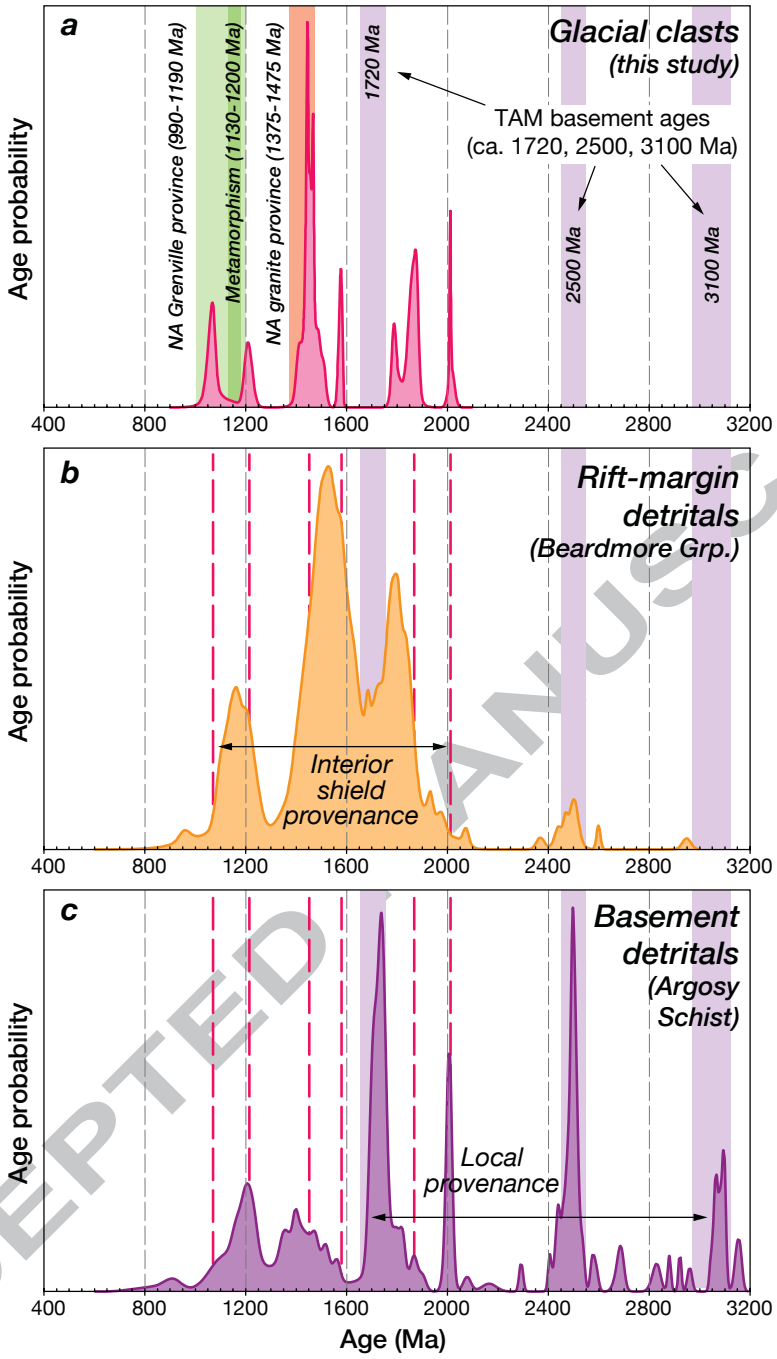

Goodge et al. [Fig. 17]

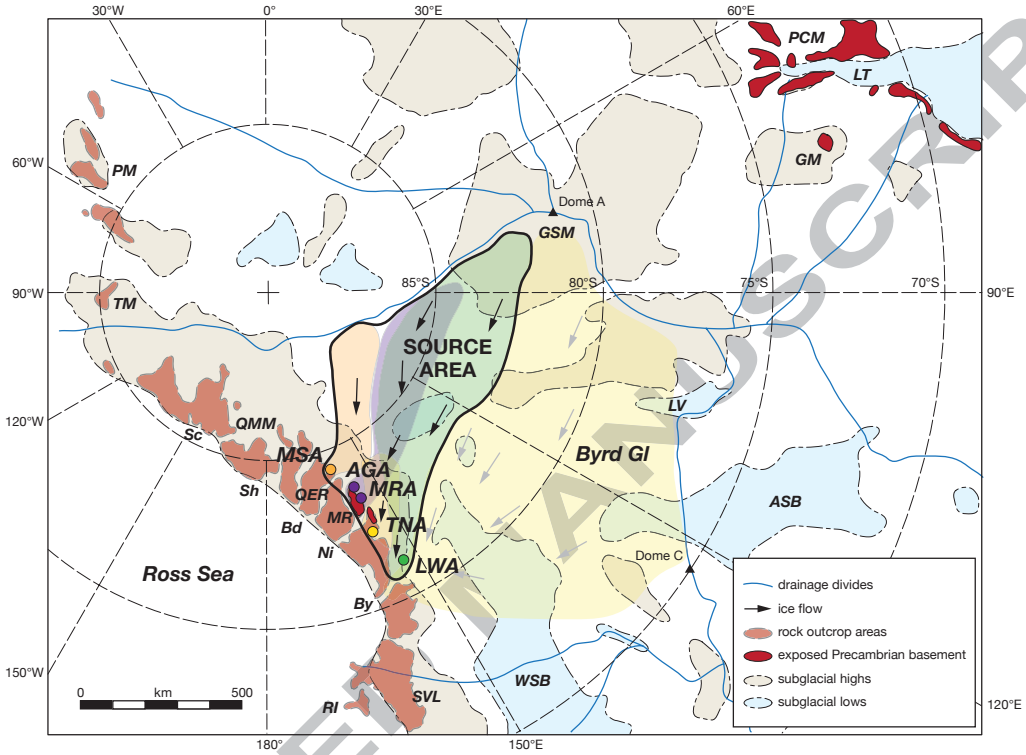

Goodge et al. [Fig.18]

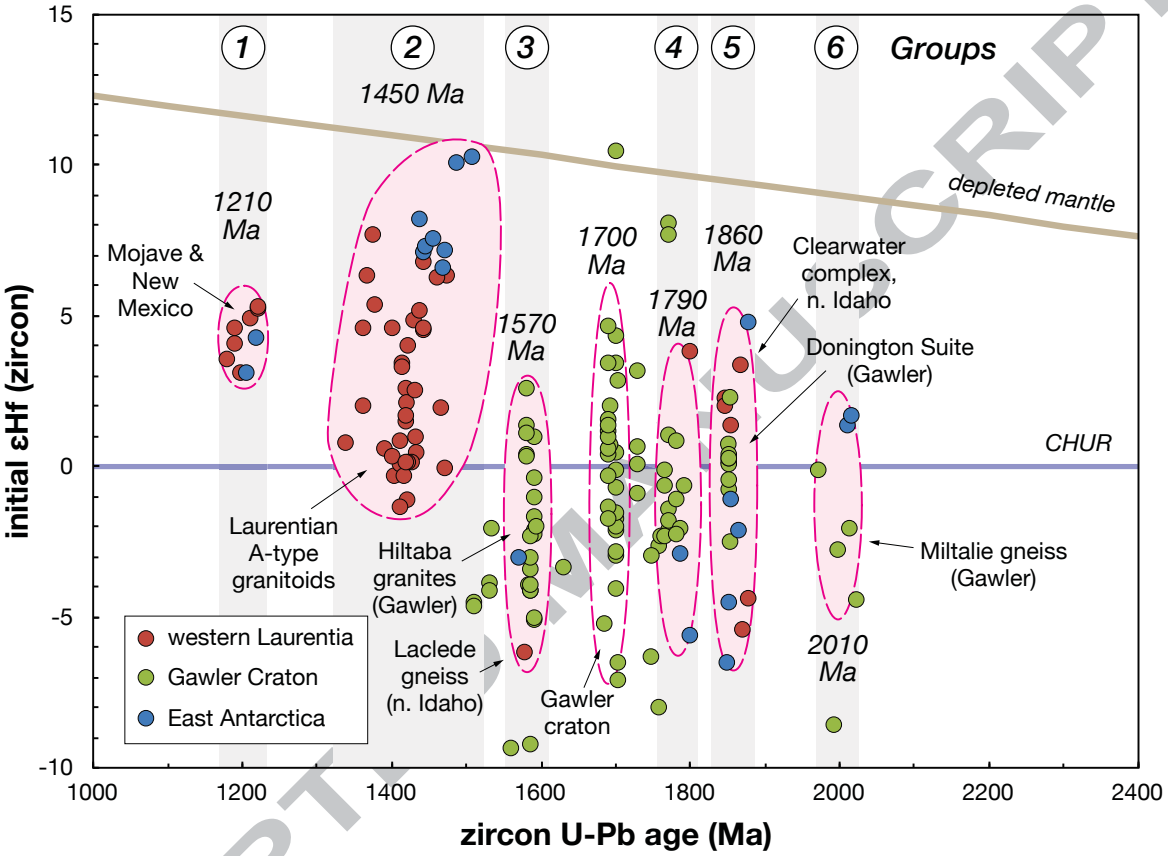

Goodge et al. [Fig. 19]

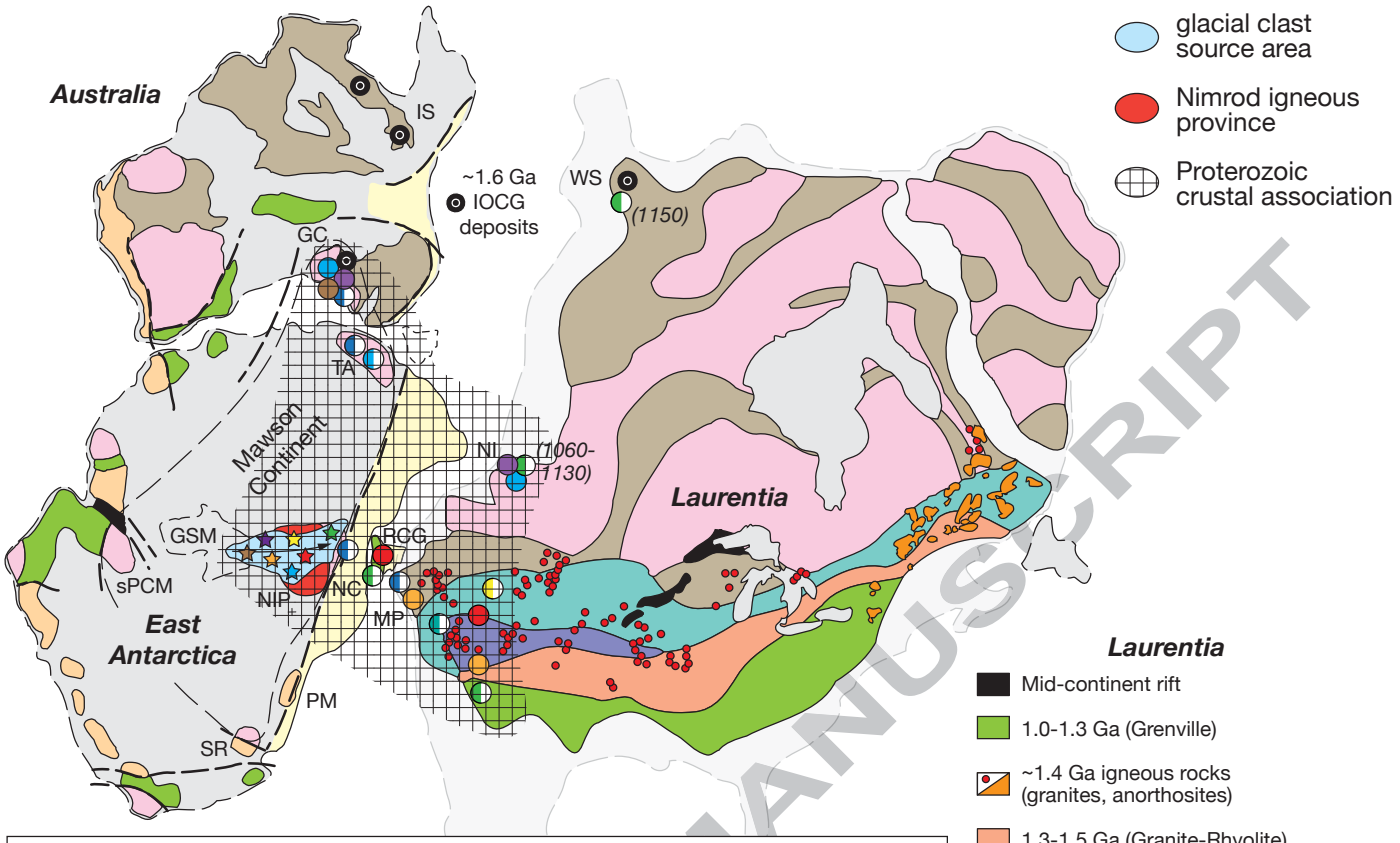

Key crustal correlations

gc = glacial clasts
dz = detrital zircons
be = basement exposure

Clast age	Isotopic + age correlation	Age correlation	Age (Ma)	Correlation source	Geological correlation
★	●	◐	1060 Ma	gc, dz	Grenville Orogen
★	●	◐	1210 Ma	gc, dz	AMCG igneous suites
★	●	◐	1450 Ma	gc, dz	A-type granite province
★	●	◐	1570 Ma	gc, dz	Gawler Craton, Laclede gneiss
	●	◐	~1.7 Ga	dz, be	Mojave Province, Gawler Craton
★	●	◐	1790 Ma	gc, dz	Yavapai-Mazatzal provinces
★	●	◐	1850 Ma	gc, dz	Clearwater complex, Gawler Craton
★	●	◐	2010 Ma	gc	Gawler Craton

Goodge et al. [Fig. 20]

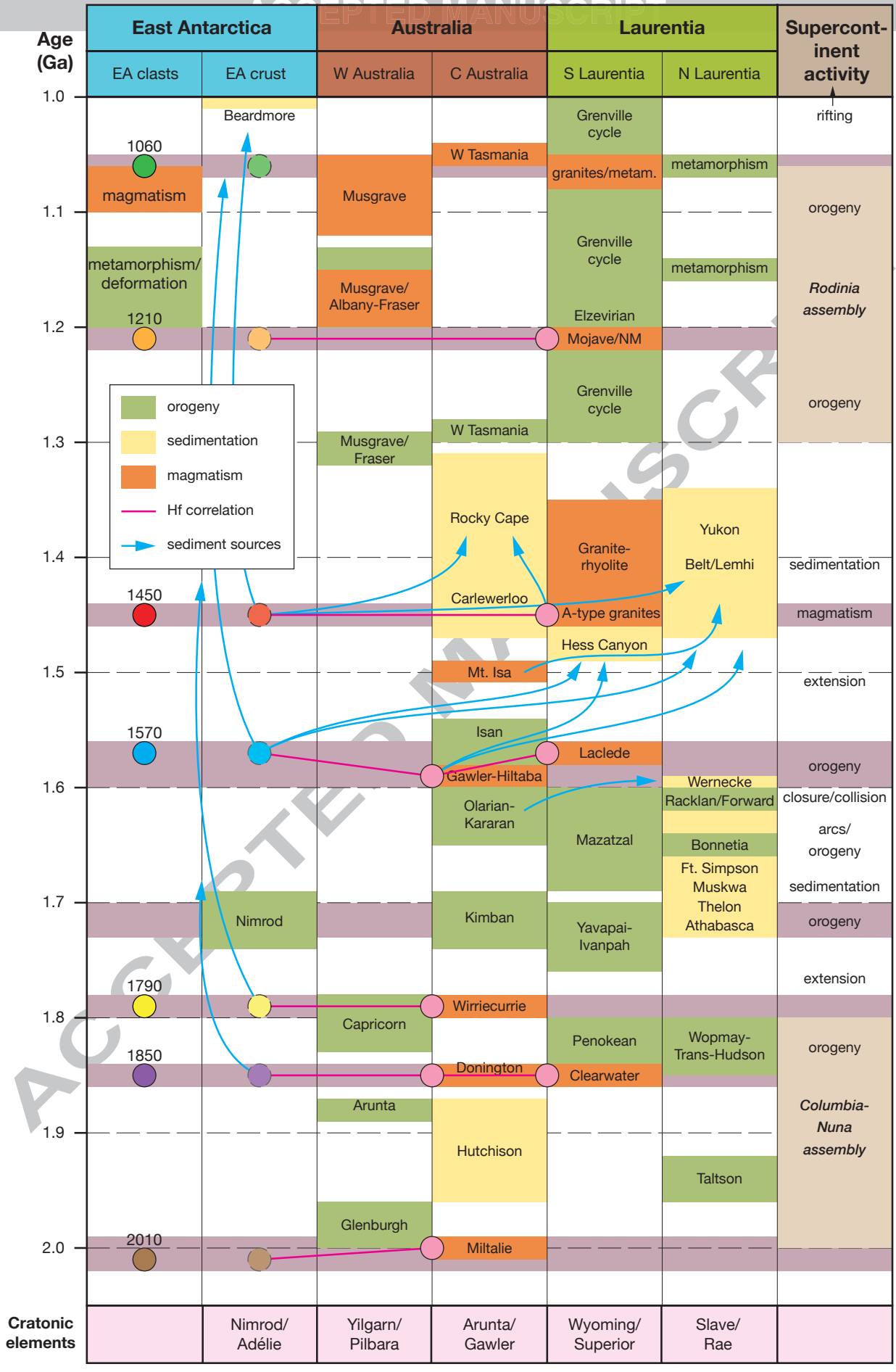

Goodge et al. [Fig. 21]

Table 1. Summary of SHRIMP U-Pb age results and isotopic data for igneous glacial clasts from Transantarctic Mountains moraines.

Sample No.	Rock type	Location	Latitude	Longitude	Magnetic susceptibility	U-Pb age	±	Age interpretation	$\delta^{18}O$	εHf (i)	T(DM)
					(10^3 SI)	(Ma)			(‰)		(Ga)
Goodge et al. (2008)											
TNQ	red A-type Ms-Bt granite	Turret Nunatak	82°25.942'S	158°07.239'E	nd	1441	6	Mesoproterozoic igneous crust	—	7.1	1.51
Goodge et al. (2010)											
AGG	Grt-Bt orthogneiss	Argo Glacier	83°29.710'S	156°44.470'E	nd	1057	12	Grenvillian igneous protolith	—	—	—
AGD	Sil-Crd-Grt-Bt orthogneiss	Argo Glacier	83°29.710'S	156°44.470'E	nd	1064	24	Grenvillian igneous protolith	—	—	—
MRV	Bt orthogneiss	Milan Ridge	83°16.985'S	156°02.240'E	nd	1070	9	Grenvillian igneous protolith	—	—	—
MRH	Sil-Grt-Bt orthogneiss	Milan Ridge	83°16.985'S	156°02.240'E	nd	1103	58	Grenvillian igneous protolith	—	—	—
LW2-18	red granite	Lonewolf Nunataks	81°19.707'S	153°09.955'E	nd	1459	6	Mesoproterozoic igneous crust	—	—	—
LW2-03	deformed granite	Lonewolf Nunataks	81°19.707'S	153°09.955'E	nd	1578	5	Mesoproterozoic igneous crust	—	—	—
LWE	granitoid	Lonewolf Nunataks	81°19.707'S	153°09.955'E	nd	1878	7	Paleoproterozoic igneous crust	—	—	—
This study											
Group 1											
10LWA-13.1	Ms-Bt granite	Lonewolf Nunataks	81°20.186'S	152°42.461'E	bd	1204	12	Grenvillian igneous protolith	7.4	3.1	1.60
10LWA-11.1	porphyritic Bt granite	Lonewolf Nunataks	81°20.186'S	152°42.461'E	1.6	1213	14	Grenvillian igneous protolith	5.8	4.3	1.57

Group 2											
10MSA-2.3	Bt leucogranite	Mt. Sirius	84°07.976'S	163°15.121'E	0.3	1410	10	Mesoproterozoic igneous crust	8.2	—	—
10TNA-1.1	rapikivi Bt granite	Turret Nunatak	82°26.018'S	158°07.349'E	0.9	1430	16	Mesoproterozoic igneous crust	7.2	8.2	1.52
10LWA-6.5	Ms-Bt granite	Lonewolf Nunataks	81°20.186'S	152°42.461'E	bd	1432	10	Mesoproterozoic igneous crust	5.0	—	—
10LWB-4.3	mylonitic Grt-Bt granite orthogneiss	Lonewolf Nunataks	81°19.545'S	153°01.445'E	bd	1448	5	Mesoproterozoic igneous crust	4.7	7.3	1.58
10LWA-6.6	foliated, annealed Ms-Bt granite	Lonewolf Nunataks	81°20.186'S	152°42.461'E	nd	1452	6	Mesoproterozoic igneous crust	—	—	—
10LWA-9.2	mylonitic Bt granite	Lonewolf Nunataks	81°20.186'S	152°42.461'E	nd	1456	7	Mesoproterozoic igneous crust	4.1	7.6	1.58
10LWA-9.3	porphyritic Bt granite	Lonewolf Nunataks	81°20.186'S	152°42.461'E	nd	1467	6	Mesoproterozoic igneous crust	4.4	6.6	1.63
10LWB-3.8	Bt granite porphyry	Lonewolf Nunataks	81°19.545'S	153°01.445'E	bd	1470	7	Mesoproterozoic igneous crust	4.6	7.2	1.62
10LWA-20.1	porphyritic Bt granite	Lonewolf Nunataks	81°20.186'S	152°42.461'E	bd	1486	8	Mesoproterozoic igneous crust	4.6	10.1	1.47
10MSA-3.5	foliated Ms-Bt leucogranite	Mt. Sirius	84°07.976'S	163°15.121'E	6.0	1508	12	Mesoproterozoic igneous crust	5.1	10.3	1.49
Group 3											
10LWA-6.4	foliated Ms-Bt granite	Lonewolf Nunataks	81°20.186'S	152°42.461'E	bd	1570	10	Mesoproterozoic igneous crust	8.1	-3.0	2.17
Group 4											
10LWA-14.1	veined Bt granite	Lonewolf Nunataks	81°20.186'S	152°42.461'E	bd	1786	8	Paleoproterozoic igneous crust	5.8	-2.9	2.33
10MRA-2.1	Grt-Bt granite orthogneiss	Milan Ridge	83°17.196'S	156°04.200'E	nd	1798	17	Paleoproterozoic igneous crust	3.8	-5.6	2.43
Group 5											
10LWB-4.5	foliated Bt granite	Lonewolf Nunataks	81°19.545'S	153°01.445'E	33.2	1848	13	Paleoproterozoic igneous crust	8.3	-6.5	2.54
10LW	layered	Lonew	81°20.1	152°42.4	bd	18	3	Paleoproter	7.1	-4.5	2.48

A-6.3	Bt granite	olf Nunataks	86'S	61'E		50	1	ozoic igneous crust			
10LWA-7.1	mylonitic Grt-Hbl-Bt granodiorite	Lonewolf Nunataks	81°20.186'S	152°42.461'E	22.8	1854	11	Paleoproterozoic igneous crust	7.1	-1.1	2.30
10LWB-4.1	foliated porphyritic Ms-Bt granite	Lonewolf Nunataks	81°19.545'S	153°01.445'E	19.1	1865	9	Paleoproterozoic igneous crust	7.6	-2.1	2.37
10MSA-3.3	foliated Bt granite	Mt. Sirius	84°07.976'S	163°15.121'E	nd	1876	11	Paleoproterozoic igneous crust	6.6	4.8	2.04
Group 6											
10LWA-10.1	foliated Hbl-Bt granite	Lonewolf Nunataks	81°20.186'S	152°42.461'E	bd	2010	3	Paleoproterozoic igneous crust	3.9	1.4	2.30
10LWA-8.1	Grt-Hbl-Bt granodiorite orthogneiss	Lonewolf Nunataks	81°20.186'S	152°42.461'E	5.2	2015	12	Paleoproterozoic igneous crust	4.3	1.7	2.30
					bd, below detection						
					nd, not determined						

Table 2. Summary of zircon O-isotope data.

Sample	SHRIMP age (Ma)	mean $\delta^{18}O$ (‰)	± 2σ external	N
10LWA-13.1	1204	7.4	0.5	11 of 13
10LWA-11.1	1213	5.8	0.5	11
10MSA-2.3	1410	8.2	0.7	9
10TNA-1.1	1430	7.2	0.4	13
10LWA-6.5	1432	5.0	0.5	8
10LWB-4.3	1448	4.7	0.5	13
10LWA-9.2	1456	4.1	0.5	9
10LWA-9.3	1467	4.4	0.5	11
10LWB-3.8	1470	4.6	0.5	19 of 21
10LWA-20.1	1486	4.6	0.5	12
10MSA-3.5	1508	5.1	0.7	11 of 12
10LWA-6.4	1570	8.1	0.5	11
10LWA-14.1	1786	5.8	0.5	9
10MRA-2.1	1798	3.8	0.4	14 of 16
10LWB-4.5	1848	8.3	0.5	17
10LWA-6.3	1850	7.1	0.5	12
10LWA-7.1	1854	7.1	0.5	12
10LWB-4.1	1865	7.6	0.5	16 of 17
10MSA-3.3	1876	6.6	0.7	16
10LWA-10.1	2010	3.9	0.5	9
10LWA-8.1	2015	4.3	0.5	10

Table 3. Summary of zircon Hf-isotope data.

Sample	SHRIMP age (Ma)	weighted mean εHf (T)	2SE	N	MSWD	prob	present-day $^{176}Hf/^{177}Hf$	2SD	arithmetic mean initial $^{176}Hf/^{177}Hf$	2SD	T_{DM} (Ga) [1]
10LWA-13.1	1204	3.1	0.4	6	1.09	0.36	0.282119	0.000035	0.282106	0.000031	1.60
10LWA-11.1	1213	4.3	0.5	12 of 13	2.90	0.00	0.282147	0.000055	0.282128	0.000057	1.57
10TNA-1.1	1430	8.2	0.3	15	1.50	0.11	0.282130	0.000047	0.282106	0.000038	1.52
10LWB-4.3	1448	7.3	0.3	14	1.50	0.13	0.282104	0.000045	0.282072	0.000039	1.58
10LWA-9.2	1456	7.6	0.3	14	0.62	0.84	0.282099	0.000023	0.282071	0.000020	1.58
10LWA-9.3	1467	6.6	0.4	12	2.40	0.01	0.282068	0.000040	0.282037	0.000036	1.63
10LWB-3.8	1470	7.2	0.6	6	1.15	0.33	0.282074	0.000035	0.282047	0.000044	1.62
10LWA-20.1	1486	10.1	0.6	9	1.40	0.20	0.282153	0.000045	0.282126	0.000045	1.47
10MSA-3.5	1508	10.3	0.3	18	0.93	0.54	0.282157	0.000038	0.282115	0.000038	1.49
10LWA-6.4	1570	-3.0	0.4	10	0.54	0.80	0.281738	0.000060	0.281701	0.000047	2.17
10LWA-14.1	1786	-2.9	0.4	9 of 11	0.95	0.47	0.281594	0.000039	0.281566	0.000033	2.33
10MRA-2.1	1798	-5.6	0.5	12 of 14	2.00	0.02	0.281524	0.000091	0.281478	0.000052	2.43
10LWB-4.5	1848	-6.5	0.6	9 of 11	2.80	0.03	0.281475	0.000056	0.281423	0.000051	2.54
10LWA-6.3	1850	-4.5	0.3	15	1.18	0.28	0.281531	0.000049	0.281466	0.000033	2.48
10LWA-7.1	1854	-1.1	0.4	15	2.50	0.09	0.281599	0.000046	0.281573	0.000047	2.30
10LWB-4.1	1865	-2.1	0.3	16	1.80	0.03	0.281558	0.000045	0.281532	0.000041	2.37
10MSA-3.3	1876	4.8	0.4	12	1.20	0.27	0.281755	0.000047	0.281722	0.000032	2.04
10LWA-10.1	2010	1.4	0.6	8	2.20	0.03	0.281609	0.000057	0.281545	0.000048	2.30
10LWA-8.1	2015	1.7	0.5	13	1.70	0.07	0.281589	0.000043	0.281546	0.000040	2.30

[1] Zircon depleted-mantle Hf model ages (T_{DM}) were calculated assuming $^{176}Lu/^{177}Hf = 0.009$ for the first stage of evolution. We adopted the CHUR parameters of Bouvier et al. (2008) and the ^{176}Lu decay constant of Söderlund et al. (2004). We used a linear depleted mantle model, assuming mantle extraction from CHUR at 3.8 Ga, with a present-day $^{176}Hf/^{177}Hf = 0.283238$ ($\varepsilon_{Hf} = +16$) and $^{176}Lu/^{177}Hf = 0.039755$ (Vervoort et al., 2016b).

Proterozoic crustal evolution of central East Antarctica:

Age and isotopic evidence from glacial igneous clasts,

and links with Australia and Laurentia

John W. Goodge [1]*, C. Mark Fanning[2], Christopher M. Fisher[3]† and Jeffrey D. Vervoort[3]

[1] Department of Earth and Environmental Sciences, University of Minnesota, Duluth, MN 55812 USA
(correspondence: jgoodge@d.umn.edu)

[2] Research School of Earth Sciences, Australian National University, Canberra, ACT 0200 Australia
(mark.fanning@anu.edu.au)

[3] School of the Environment, Washington State University, Pullman, WA 99164, USA
(vervoort@wsu.edu, cmfisher@ualberta.ca)

Highlights

- Glacial igneous clasts provide a novel means of assessing the interior geology of ice-covered East Antarctica.
- Granitoid clasts eroded from central East Antarctica show that the crust in this region was formed by a series of magmatic events at ~2.01, 1.88-1.85, ~1.79, ~1.57, 1.50-1.41, and 1.20-1.06 Ga.
- The dominant granitoid populations are ca. 1.85, 1.45 and 1.20-1.06 Ga, but none of these igneous ages are known from the limited outcrop in the region.
- Age and O-Hf isotopic data indicate the presence of a large, composite Proterozoic igneous province in cratonic East Antarctica, and they correlate with crust in both the Gawler Craton of present-day Australia and Proterozoic provinces in southwestern Laurentia.
- Abundant ~1.2-1.1 Ga igneous and metamorphic clasts may indicate the presence of a Mesoproterozoic orogenic belt underlying the Gamburtsev Subglacial Mountains.